

Sl. No.	<p style="text-align: center;"><b>IIT Ropar</b>  <b>List of Recent Publications with Abstract</b>  <b>Coverage: August, 2025</b></p>
A	<p style="text-align: center;"><b>Conference Proceeding(s)</b></p>
1.	<p><a href="#">A brief review of state-of-the-art classification methods on benchmark peripheral blood smears datasets</a>  <b>MS Kanroo, HS Kawoosa, Tanushri, M Aggarwal, P Goyal</b> - International Conference on Computer Vision and Image Processing (CVIP 2025), 2024</p> <p><b>Abstract:</b> White blood cells (WBCs) play a crucial role in the immune system, with their morphology and subtype counts serving as key indicators for diagnosing conditions like anemia and leukemia. However, manual WBC classification in peripheral blood smears is time-consuming, highlighting the need for automated WBC classification systems. Recent advancements in deep learning, including convolutional neural networks and vision transformers, have demonstrated significant potential in medical imaging by effectively extracting meaningful features. This paper surveys state-of-the-art techniques, examining relevant datasets and WBC types. We conduct a comprehensive performance analysis of nine models on two benchmark datasets, BCCD and PBC. Our findings indicate that ConvNeXt achieves a weighted average accuracy (WAA) of 89.58% and an F1-Score of 90.00% on the BCCD dataset, while DenseNet demonstrates superior performance on the PBC dataset, with a WAA of 98.88% and an F1-Score of 98.88%.</p>
2.	<p><a href="#">Bluetooth low energy antenna design for monitoring applications</a>  <b>R Raina, KJ Singh, S Kumar</b> - 2025 10th International Conference on Smart and Sustainable Technologies (SpliTech), 2025</p> <p><b>Abstract:</b> Bluetooth technology enables short range data exchange between the devices. It operates in 2.4 GHz Industrial, Scientific and Medical (ISM) band, allowing connectivity for devices such as smartphones, headphones and Internet of Things (IoT) applications. Several bluetooth antennas have been discussed previously but they come with some limitations, i.e. some are large in size, some have less bandwidth percentage and some have less gain. Therefore, small sized bluetooth antenna is proposed in the paper with 15 mm radius and 1.6 mm thickness using Roger RT duroid 5880 substrate. The proposed compact bluetooth low energy antenna possess simulated bandwidth percentage of 4.08 %, 2.03 dBi gain and 99.20 % radiation efficiency. Moreover, the simulations were done using Ansys High Frequency Structure Simulator (HFSS) software.</p>
3.	<p><a href="#">Circularly polarised RFID reader antenna with an integrated power divider</a>  <b>R Raina, KJ Singh, S Kumar</b> - 2025 10th International Conference on Smart and Sustainable Technologies (SpliTech), 2025</p> <p><b>Abstract:</b> In modern times, Ultra High Frequency (UHF) Radio Frequency Identification (RFID) systems have been widely utilized for tracking across various applications, including human surveillance, healthcare, library management, inventory control and the Internet of Things (IoT). Various antennas have been developed for RFID applications in previous studies; however, they come with certain limitations. Some exhibit a lower bandwidth percentage, while others have reduced gain. To address these issues, this paper proposes an RFID reader antenna with enhanced gain. The proposed RFID antenna operates within the 846 - 950 MHz frequency band, offering a 11.58 % bandwidth and a gain of 9.05 dBi. Additionally, it possesses 1.2 dB axial ratio and is circularly polarised. The antenna design includes an aluminium ground measuring 296 mm x 296 mm x 1.6 mm and a stainless steel patch with 165 mm x 146 mm x 0.8 mm dimensions. The designed antenna is analysed through simulations using Ansys High Frequency Structure Simulator (HFSS).</p>

4.	<p><a href="#">ConvSFNet: A novel architecture for disaster image analysis</a>  B Debnath, K Kumawat, P Dey - International Conference on Computer Vision and Image Processing, 2024</p> <p><b>Abstract:</b> The proper classification of social media images in a timely manner is a very critical component of how effective response and recovery operations would be in a disaster ridden scenario. This paper enunciates ConvSFNet as a new architecture for disaster image classification, where ConvNeXt has been combined with the Squeeze-and-Excitation block and the Feature Pyramid Network structure. Using the MEDIC dataset, thorough experiments were conducted with models like DenseNet121, EfficientNet-B1, ResNet50, SqueezeNet, and VGG16 for performance comparison. All our results outperform the baseline models on accuracy, weighted precision, recall, and F1-score on all four classification tasks: Damage Severity, Disaster Type, Humanitarian, and Informative. ConvSFNet improved the average F1-score by 2.41%, excelling in the “severe” damage category, very relevant in scenarios of disaster management. This research points to the effectiveness of integrating SE blocks and FPN to improve feature extraction and classification in disaster image analysis. These results illustrate the great promise ConvSFNet holds for real-time disaster response and management by opening further paths for future research in this domain.</p>
5.	<p><a href="#">Cyclic response of natural rubber latex treated Sutlej sand under stress controlled loading</a>  S Sharma, N James - Dynamic Soil Properties and Liquefaction (ICRAGEE 2024), 2025</p> <p><b>Abstract:</b> Investigating the site-specific mechanical behavior of sand under cyclic loading holds crucial importance in geotechnical and many other engineering applications. The Sutlej River sand has been used in the present study because of its high liquefaction susceptibility, as the Sutlej River lies in the high-risk seismic zone in the northeastern part of the Punjab state. The comparative study between the in situ Sutlej River procured sand and Natural rubber latex (NRL) treated Sutlej sand has been done by employing stress-controlled cyclic triaxial tests under varying experimental conditions. The testing has been performed over different confining pressures under varying material circumstances, i.e., different concentrations of permeated NRL solution and relative densities. The number of cycles required for onset of liquefaction has been investigated using the cyclic triaxial test. It has been shown by testing that the number of cycles necessary for the onset of liquefaction increased with an escalation in the relative density and NRL concentration. The present study reveals that introducing NRL into the sand is an efficient technique for improving the mechanical behavior of sand under cyclic loading. Therefore, the NRL permeation technique can be used as an effective liquefaction mitigation measure for the locally available sands.</p>
6.	<p><a href="#">Development of self-lubricating copper metal matrix hybrid composites using microwave sintering and its characterizations</a>  MK Singh...H Nautiyal...G Ji - Recent Advances in Functional Materials, Volume 1: Select Proceedings of RAFM 2024, 2025</p> <p><b>Abstract:</b> Copper is one of the highest uses of metal as electrical contact where a continuous relative motion occurs, which leads to its deterioration and stops functioning. Therefore, it requires good strength and sliding resistance during its mating. So, this work is primarily emphasized on the synthesis of new copper metal matrix hybrid composites using the advanced microwave sintering (MWS) technique, where hard zirconia (<math>ZrO_2</math>) and soft molybdenum disulfide (<math>MoS_2</math>), including chromium (Cr), were reinforced in the matrix of copper. There were three copper metal matrix hybrid composites developed by microwave sintering according to the different weight percentages (wt.%) of reinforcements and designated as MWS-HC-1, MWS-HC-2, and MWS-HC-3. The high-resolution scanning electron microscope (HRSEM), high-resolution X-ray diffraction (HRXRD), and energy-dispersive analysis of X-rays (EDAX), including the elemental color mapping, were utilized to characterize the synthesized copper-based hybrid composites. The electrical conductivity of synthesized hybrid composites was also investigated and revealed no significant loss in electrical conductivity of copper on the ceramic reinforcements. HRXRD,</p>

	<p>HRSEM, and EDAX, including elemental color mapping analysis, exposed the reinforcing particles' presence and its fair distribution in the copper matrix with its superior interfacial bonding. The experimental density of the synthesized hybrid composites was also evaluated and found that it was decreasing with increasing content of reinforcements. The wear test was performed for the developed hybrid composites using pin-on-disk arrangement under dry conditions. The friction coefficient and weight loss were decreasing as the reinforcement content increased. It is possible due to the self-lubricating action of the MoS<sub>2</sub> reinforcements in the matrix.</p>
7.	<p><a href="#">Enhancing UAV network security: Machine learning for DDoS attack detection</a>  <b>I Sharma, S Agarwal, SS Jha</b> - 2025 10th International Conference on Smart and Sustainable Technologies (SpliTech), 2025</p> <p><b>Abstract:</b> Assaults on network components and devices are a major threat to network services. Therefore, new technical solutions need to be developed to counter these attacks and improve the efficiency of attack detection systems. This paper presents a Distributed Denial of Service (DDoS) attack detection algorithm for mobile Unmanned Aerial Vehicles (UAV) networks. We consider a Software Defined Networks architecture and propose a Machine Learning (ML) based attack detection module. By incorporating novel features such as flow count, speed of source IP, source IP address entropy, destination IP address entropy, etc., in our ML-based model, we show that the detection performance significantly increases in the UAV networks. ML algorithms used are Random Forest, Multi-Layer Perceptron, and Support Vector Machine. The performance has been evaluated under varying traffic types (TCP, UDP, and ICMP) and attack traffic intensities (light and heavy). In comparison to the state-of-the-art schemes having an accuracy of approximately 95%, our proposed scheme achieves an average accuracy of around 99%. Our current work paves the way for the development of an efficient attack mitigation system in mobile UAV networks.</p>
8.	<p><a href="#">Influence of grain size on formability in micro-incremental sheet forming</a>  <b>M Pal, A Agrawal, CK Nirala</b> - Micro Manufacturing: Proceedings of the AIMTDR 2023, 2025</p> <p><b>Abstract:</b> Micro-incremental sheet forming (<math>\mu</math>ISF) is a flexible manufacturing process and has advantages over existing micro-forming processes, due to its die-less nature of material deformation. In <math>\mu</math>ISF, an ultra-thin foil is plastically deformed into a complex 3D geometry. It is precisely governed by the pre-defined toolpath of the forming tool on the surface of the foil. Due to size-effect, achieving high formability of the foils in micro-forming is difficult. This work investigates the deformation behavior of 100 <math>\mu</math>m thick CP-Ti Gr2 foils. The received foil is heat-treated at two different temperatures to obtain the foils with altered grain sizes. It was witnessed that the changes in annealing temperature and grain size enhanced the formability of the micro-parts. The foil with a higher grain size helped in increasing the fracture limit of the formed components.</p>
9.	<p><a href="#">Intelligent analog and mixed-signal IC (I-AMS-IC) design: A conceptual framework, and case study on AI integration</a>  <b>N Sharma, A Pratap, DM Das</b> - 2025 Seventh International Symposium on Computer, Consumer and Control (IS3C), 2025</p> <p><b>Abstract:</b> A conceptual framework, I-AMS-IC (Intelligent Analog and Mixed-Signal IC), is proposed to enable automation in analog/mixed-signal (AMS) design by integrating machine learning with an emphasis on interpretability and trustworthiness. The framework is demonstrated using a custom-built dataset based on an operational amplifier (Op-Amp) case study. Machine learning models are trained to predict design variables from ten key performance indicators (KPIs). The relationships between design variables and performance metrics are explored using various correlation analysis methods. Among the models tested, XGBoost regression achieves the best performance with a mean absolute percentage error (MAPE) of 16.88%. To enhance interpretability, SHAP (Shapley Additive Explanations) is employed to explain model predictions. The SHAP insights are validated through both correlation analysis and analytical circuit expressions. The study highlights that combining statistical, analytical, and explainability</p>

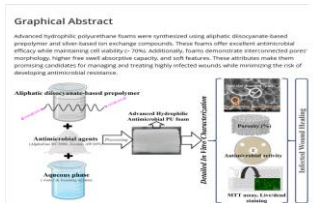
	<p>techniques strengthens trust and transparency in AI-assisted AMS design, paving the way for more interpretable and automated design workflows.</p>
10.	<p><a href="#">Investigation of combustion stability in an RCCI engine using recurrence analysis of cylinder pressure data</a>  <b>KS Kumar, R Prashar, RK Maurya</b> - Recurrence Plots and Their Quantifications: Methodological Breakthroughs and Interdisciplinary Discoveries: Proceedings of the 10th International Symposium on Recurrence Plots (ISRP 2023), 2023</p> <p><b>Abstract:</b> The Reactivity Control Compression Ignition (RCCI) engines offer better emission control and thermal efficiency compared to conventional diesel engines. However, cyclic variations leading to engine combustion instability pose a significant challenge in their development and commercialization. This study aims to identify the engine configuration with superior deterministic traits by implementing recurrence analysis techniques (recurrence plot and its quantifications) on Indicated Mean Effective Pressure (IMEP) time series data obtained from a modified single-cylinder diesel engine. Experiments were conducted with varying engine configurations, including different load conditions (4 kg and 8 kg), diesel direct injection mass split ratio (50–50 and 70–30), and port fuel injection mass (8 mg/cycle and 12 mg/cycle), all while advancing diesel main injection timings (SOI-2: 10°, 20°, 30°, 40°, and 50° bTDC). The analysis demonstrated that the combustion process exhibited RCCI mode only when the main injection timings were from the onset of intermediate SOI-2. Based on the recurrence plot (RP) and its quantification analysis (RQA) conducted for these operating conditions, this study concludes that the engine when operating at SOI-2 40° bTDC, 70–30 DIMR, and 12 mg/cycle PFI mass, exhibits superior deterministic traits compared to the other tested configurations. Identifying such configurations would facilitate the implementation of an effective engine control strategy for stabilized RCCI engine operation.</p>
11.	<p><a href="#">Liquefaction mitigation using natural rubber latex treatment</a>  <b>U Veena, N James</b> - Dynamic Soil Properties and Liquefaction: Select Proceeding of the 8<sup>th</sup> ICORAGEE, 2024, 2025</p> <p><b>Abstract:</b> Pertaining to the loose cohesionless soil deposits, the primary concern of geotechnical professionals is liquefaction failure. Hence, liquefaction mitigation has become a prime objective of ground improvement research. Most of the liquefaction countermeasures are developed with a focus on modifying factors such as plasticity, density, size and shape of particles, saturation degree, etc. This study presents a novel method for liquefaction mitigation in sands using natural rubber latex (NRL) treatment. The commercially available Quartzanium grade III sand was used for cyclic response and liquefaction studies. The strain-controlled cyclic triaxial tests with a frequency of 1 Hz and shear strain amplitudes of 0.225, 0.45, and 0.75% were performed to assess the liquefaction resistance and modulus degradation. The NRL-treated samples were prepared using a pressurized permeation method to permeate ready-prepared sand samples with NRL solutions of concentrations ranging from 10 to 30%. The study considered a unit value of pore pressure ratio to indicate the onset of liquefaction. The outcomes of strain-controlled cyclic triaxial tests showed that the NRL treatment effectively lowers the pore pressure build-up and prevents liquefaction. The performance of the treated sand improved with an increase in the concentration of NRL solution used for the treatment.</p>
12.	<p><a href="#">MalVIS: A pyramid vision transformer V2 (PVTv2) based framework for android malware detection</a>  <b>Devnath, MM Sikhwal, B Subba</b> - 2025 34th International Conference on Computer Communications and Networks (ICCCN), 2025</p> <p><b>Abstract:</b> This paper proposes MalVIS, an android malware detection framework based on pyramid vision transformers V2(PVTv2). MalVIS leverages the hierarchical self-attention mechanism of (PVTv2) to enhance detection of android based malware binaries. The pyramid structure of MalVIS enables it to efficiently capture the fine-grained and high-level features. It</p>



	<p>employs Spatial Reduction Attention (SRA) to reduce computational complexity by decreasing the number of tokens at each stage, which makes it suitable for deployment on resource-constrained environments. Additionally, MalVIS benefits from convolutional feed-forward networks (FFNs) to improve feature representation for effective malware classification. Experimental analysis on the benchmark MALNET-IMAGE dataset shows that MalVIS outperforms many state-of-the-art android malware detection frameworks, such as ViT-B Sherlock, ResNet, DenseNet, and MobileNetV2. It achieves an F1-score of 0.965 (binary classification) and 0.724 (multi-class classification) on the MALNET-IMAGE dataset.</p>
13.	<p><a href="#">MSPlantNet: Plant disease classification using few shot learning</a>  <b>R Chakraborty, MS Anis, P Kumar, MK Jha, N Goel, M Saini</b> - International Conference on Computer Vision and Image Processing (CVIP 2024), 2025</p> <p><b>Abstract:</b> Accurate diagnosis of plant diseases is vital for crop survival and growth directly influencing the agricultural economy. However, the limited availability of plant pathology specialists presents a significant challenge. This research proposes an automated system utilizing advanced deep learning techniques to identify plant diseases from images. Traditional deep learning models often require large datasets, which are typically unavailable due to their limited coverage and different sample sizes for various diseases. To address this a Meta Learning approach specifically Few Shot Learning has been applied which excels in scenarios with limited data by rapidly adapting to new classes with minimal samples. Furthermore, a Multi-scale architecture has also been implemented to enhance feature extraction and improve performance on small datasets. The proposed approach demonstrates substantial improvements in accurately diagnosing plant diseases with limited data, offering a practical solution for farmers to reduce economic losses caused by undiagnosed or misdiagnosed plant conditions.</p>
14.	<p><a href="#">Precision in contactless respiratory monitoring: Machine learning-based algorithm performance</a>  <b>A Hari, H Arora...B Kumbhani, S Darshi, S Agarwal, JS Sahambi...</b> - 2025 10th International Conference on Smart and Sustainable Technologies (SpliTech), 2025</p> <p><b>Abstract:</b> Respiratory monitoring is crucial for patient care, especially for infants, providing essential data for diagnosing and managing various health conditions. Traditional methods often lack the precision and real-time capabilities required for optimal outcomes. This study evaluates the performance of machine learning (ML) based algorithms for the automation of contactless respiration monitoring to reduce the manual intervention of medical experts in predicting the health condition of neonates in the neonatal intensive care unit (NICU). Particularly, the random forest algorithm is used in this work for enhancing precision in respiratory monitoring. This algorithm is known for its robustness and ability to handle complex, non-linear relationships and aggregate predictions from multiple decision trees to improve accuracy. This research involves analyzing extensive patient data, especially respiratory rate, to train and validate the algorithm. Preliminary results indicate that the proposed ML-based algorithm significantly improves the precision of respiratory monitoring and offers a promising tool for healthcare providers. This study highlights the potential for machine learning to transform patient care monitoring.</p>
15.	<p><a href="#">Radio frequency identification reader antenna design for tracking applications</a>  <b>R Raina, KJ Singh, S Kumar</b> - 2025 10th International Conference on Smart and Sustainable Technologies (SpliTech), 2025</p> <p><b>Abstract:</b> Radio Frequency Identification (RFID) is the technology employed for automatically identifying and tracking animals, things or people using radio waves. Therefore, several antennas designed for RFID applications have been introduced in the previous literature works. But they possess some drawbacks. For example, some have less bandwidth percentage and some have less gain. Thus, this paper introduces a high gain RFID reader antenna. The proposed RFID antenna works in 846 - 930 MHz frequency band with 9.45 % bandwidth percentage and 9.09 dBi gain. Moreover, the proposed antenna has circular polarisation and has 2.07 dB axial ratio. The antenna presented features an aluminium ground measuring 296 mm x 296 mm x 1.6 mm and a stainless</p>

	<p>steel patch with dimensions of 146 mm x 141 mm x 0.8 mm. The proposed design has been simulated on Ansys High Frequency Structure Simulator (HFSS).</p>
16.	<p><a href="#">Transformation of vehicular networks through machine learning: Challenges and opportunities</a>  <b>SK Singh, N Gupta, A Hari, R Singh, B Kumbhani</b> - 2025 10th International Conference on Smart and Sustainable Technologies (SpliTech), 2025</p> <p><b>Abstract:</b> Autonomous vehicles (AVs) are currently getting widespread attention and considered as a highly promising application of wireless communication. Due to the standout features of 5G/6G, it is capable of supporting V2X (Vehicular to Everything) communications and can fulfill the communication requirements. For the efficient vehicular ad-hoc network (VANET), lower latency and ultra-reliability are prime requirements. Next, larger handoffs, high interference, and dynamic traffic are the major obstacles to seamless connectivity. These issues can be effectively tackled through the concept of Machine Learning (ML). In this paper, we conduct a comprehensive survey of vehicular communication, discussing its major challenges, highlighting the transformative potential of ML algorithms, and addressing the implementation challenges of ML for creating a smooth vehicular network. Furthermore, we explore future research opportunities in this direction.</p>
<b>B</b>	<b>Article(s)</b>
17.	<p><a href="#">A reconfigurable SWIPT antenna array for battery assisted cooperative relaying in IoT networks</a>  <b>S Kumar, A Sharma</b> - IEEE Transactions on Antennas and Propagation, 2025</p> <p><b>Abstract:</b> Cooperative relaying (CoR) is extensively utilized to extend the communication range, spectral efficiency, and system capacity. To achieve a highly reliable and sustainable CoR, the antenna system at energy-constrained relay nodes should provide broader coverage with the capability to replenish its battery. This work proposes a 2×2 reconfigurable simultaneous wireless information and power transmission (SWIPT) antenna array comprising four frequency-splitting antenna elements. A reconfigurable feed network is designed to achieve pattern and polarization reconfigurable wireless information transmission (WIT) in 5 GHz WiFi band. On the other hand, WPT is implemented at 5 GHz utilizing a completely integrated conjugate impedance-matched full wave rectification circuit. Moreover, the DC outputs of all four SWIPT antenna elements are combined in parallel to enhance the overall harvested DC power with negligible circuit losses. The performance of the proposed antenna system is validated using software-defined radio to showcase its capability to implement battery-assisted cooperative relaying in IoT networks.</p>
18.	<p><a href="#">Advanced silver ion exchange-based hydrophilic antimicrobial PU foams: Synthesis and comprehensive in vitro characterizations</a>  <b>JH Rajput, V Rathi, A Mukherjee, P Yadav, T Gupta, B Das, A Poundarik</b> - Journal of Polymer Science, 2025</p> <p><b>Abstract:</b> Chronic wounds are hard-to-heal ulcers often complicated by antimicrobial-resistant infections caused by the overuse of antimicrobial agents. Infections contribute to the refractory character of wounds, accounting for around 50% of total cases. This emphasizes the need for advanced dressing materials, such as antimicrobial foams, that can inhibit rapid and sustained bacterial growth, manage exudate, and be non-cytotoxic. In this work, hydrophilic antimicrobial polyurethane (PU) foams were developed using silver-based ion-exchange compounds and a safer aliphatic diisocyanate prepolymer, replacing commonly used less biocompatible aromatic diisocyanates. The antimicrobial agents' concentration in PU foam was optimized to ensure <math>\geq 70\%</math> cell viability and effective antimicrobial efficacy without significantly compromising their physicochemical properties. PU foams' exudate handling capacity and physical properties were evaluated according to BS EN13726 and ASTM D3574-17 standards. Foams with AlphaSan RC2000 showed better biocompatibility and antimicrobial effectiveness against Staphylococcus aureus and Pseudomonas aeruginosa than Zeomic AW10N-based foams, attributed to their elemental composition. PU foams with AlphaSan RC2000 exhibited well-interconnected pores,</p>

soft, higher free swell absorptive capacity (> 15 g/g), effective antimicrobial efficacy (> 75%–99% OD600 reduction), and biocompatibility. The detailed outcomes of in vitro characteristics collectively confirmed that AlphaSan RC2000-based PU foams could potentially be used for managing and treating infected wounds.



[Advancements in spinal cord injury treatment: integrating drug delivery, biophysical stimulation, cell-based therapies, and tissue engineering approaches](#)  
**M Bhatt, B Das - ACS Applied Bio Materials, 2025**

**Abstract:** Spinal cord injuries, whether resulting from traumatic or nontraumatic events, have severe and lasting detrimental effects on individuals, significantly impacting their overall health, mobility, and quality of life. The limited regenerative capacity of the spinal cord is mainly due to neuronal damage, the presence of inhibitory molecules, an impaired immune response, and the formation of glial scars, all of which create a hostile environment for neural repair and functional recovery. The majority of SCIs are caused by traffic accidents and falling objects. The current global treatments used for SCI are surgical methods, steroid medications, physiotherapy, and spinal cord epidural stimulations. However, these approaches offer only temporary relief and have serious adverse effects. Various preclinical approaches have been studied for SCI, including biomaterials, drug delivery, electrical stimulation, and cell-based therapies. Among these, stem cell therapies, such as NSCs, MSCs, and iPSCs, have the potential to significantly improve axonal regrowth, reduce inflammation, and promote neuroprotection. Furthermore, biophysical stimulation methods such as optogenetics, electrical and mechanical stimulation, and biomechanical devices offer encouraging paths toward improving neural plasticity and functional recovery. However, combinational approaches such as biomaterials with cell-based systems, cell-based systems with drug delivery, and biophysical stimulation with biomaterials aim to have more significant potential for functional recovery than a single treatment alone. This review has discussed the current clinical practices for SCI treatment, their limitations, and combinational strategies for spinal cord regeneration. So, this article can give clinicians, bioengineers, and researchers clues to construct preclinical and clinical studies that can have long-term effects on patients.

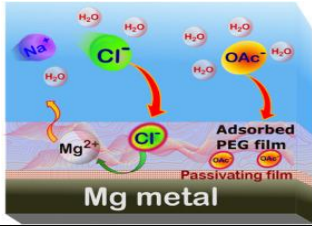
[AMORA-adaptive multi-objective routing algorithm in payment channel networks](#)  
**S Mishra, S Pal - IEEE Transactions on Network and Service Management, 2025**

**Abstract:** Blockchain offers an efficient, reliable, and secure environment for performing transactions. Scalability, high transaction fees, routing services, and low throughput are some of the primary challenges of blockchain-based cryptocurrencies. Off-chain transactions are used to tackle these challenges. Payment Channel Networks (PCNs) are developed for implementing off-chain transactions, which require routing algorithms for making successful payments between users. The existing literature proposes many routing algorithms for these transactions in PCNs. However, existing routing algorithms in PCNs considered only a single objective while performing routing. Our proposed Adaptive Multi-Objective Routing algorithm (AMORA) considers multiple objectives that enhance the cost-effectiveness, throughput, and network resiliency in PCNs. Additionally, it reduces the hop count for transactions to retain long-term sustainability. AMORA is based on a local search-based memetic algorithm (MA). MA improves routing through multi-objective optimization. Rigorous simulation evaluation demonstrates that AMORA optimizes transaction time by 31.10%, 47.2%, 46.75%, 33.47%, 48.38%, and 74.3% and increases throughput by 55.34%, 40%, 29.73%, 57.69%, 50.78%, 59.81% compared to the Fence, Dijkstra, MILPA-PCN, SpeedyMurmurs, Spider, and Flash algorithms, respectively. Furthermore, we carry out a theoretical analysis of AMORA's convergence and compute computational complexity.

21.	<p><a href="#">Analytical framework for throughput enhancement in BLE extended advertising with packet chaining</a>  <b>LK Baghel, G Shan, E Kanjo, BH Roh - IEEE Wireless Communications Letters, 2025</b></p> <p><b>Abstract:</b> Bluetooth Low Energy (BLE) 5.x introduced extended advertising with packet chaining for high-throughput BLE-based IoT applications. However, achieving maximal throughput in BLE largely depends on the selection of transmission parameters, such as packet size and the number of chained packets. Therefore, determining the optimal packet size and the number of chained packets is crucial. However, this task is challenging due to the nonlinearity of the problem. To date, none of the existing works have focused on determining the optimal values for these parameters. To address the aforementioned bottlenecks, we first develop a comprehensive analytical framework to model throughput. Based on this framework, we derive simplified closed-form analytical expressions to choose the transmission parameters optimally, ensuring maximal throughput. Additionally, we develop an algorithm that autonomously optimizes transmission parameters based on network configuration. Analytical results demonstrate that the proposed framework significantly improves throughput compared to conventional approaches. The accuracy of our analytical model is validated through simulations, demonstrating strong agreement with the analytical results.</p>
22.	<p><a href="#">Ancient Indian sustainable healthcare: Kalari Marmachikitsa, a comprehensive indigenous medical system</a>  <b>A Nandha, AV Suresh - Journal of Human Values, 2025</b></p> <p><b>Abstract:</b> Indian civilization is renowned for promoting holistic lifestyle practices that nurture environmental and genus-inclusive practices. Due to this non-anthropocentric philosophy of life ingrained in ancient Indian culture, traditional Indian medical knowledge systems are accommodative of healthy habits fostering mental and physical wellness. This article studies kalari marmachikitsa, an alternative treatment method anchored in traditional knowledge centring on the system of marmas as detailed in the ancient Indian medical text, <i>Sushruta Samhita</i>. The article explores the health benefits of this treatment and analyses this alternate treatment method as a sustainable and holistic wellness system using a qualitative study. It explores the themes of uniqueness, perception of side effects and reasons for preferring this treatment method. Through this interpretation of data, the study theorizes the aspects of sustainability rooted in kalari marmachikitsa, an indigenous healthcare knowledge system.</p>
23.	<p><a href="#">Annual short duration exploitability profiles for zonal classification of wave energy resources.</a>  <b>S Roy - Energy, 2025</b></p> <p><b>Abstract:</b> For wave energy converters to be integrated within utility network, marine resources must be exploited despite short duration variability of source waves. A conventional assessment of wave resources typically involves data at hourly (or higher) intervals with short duration variations unrepresented, and is therefore somewhat incomplete from the perspective of network integration. Further, as energy flux variability differs between seasons, a complete assessment of resource exploitability must represent all possible seasonal conditions over a year. This is largely beyond the scope of long term wave indices that have been in common use. This work introduces seasonal short duration wave exploitability profile as a linear regression over possible combinations of maximum significant wave height and short duration wave energy flux that may occur at a marine region across different seasons. Computed wave exploitability profiles are compared across Indian marine deepwaters, which facilitates distinctive zonal classification beyond conventional exploitability indices. The classification substantiates superiority of the Upper Coromandel offshore for wave energy exploitation, while deepwaters of the Arabian Sea appear to be inferior by comparison. Additionally, exploitability profiles are shown to be good supplement to assessment by long term wave models or reanalysis databases; the zonal classification being adequately robust to climate dynamics.</p>
24.	<p><a href="#">BLE 5.x-based enhanced service architecture for delay-sensitive IoT applications</a>  <b>LK Baghel, G Shan, R Singh, S Kumar, BH Roh, J Ali - IEEE Internet of Things Journal, 2025</b></p>



	<p><b>Abstract:</b> Recent advancements in Bluetooth Low Energy (BLE) have made it a promising solution for delay-sensitive and energy-constrained IoT applications, such as robotic automation in industrial settings. However, existing BLE service architectures, namely the BLE beacon-to-user and beacon-gateway-server-user models, either suffer from high delays, unreliable performance, or a reliance on internet connectivity, which is often limited in environments such as underground parking areas, airports, and supermarkets. Additionally, these architectures use BLE legacy advertising, which offers limited throughput and thus contributes to further delays. To address these limitations, this paper proposes a novel BLE-centric enhanced service architecture that minimizes the delay experienced by users and enhances the energy efficiency of BLE beacons. Based on the proposed service architecture, we first develop an analytical model to evaluate delay and then derive simplified closed-form expressions for selecting optimal transmission parameters. These parameters minimize the delay experienced by users and improve the energy efficiency of BLE beacons. The proposed architecture also leverages BLE extended and periodic advertising modes, which offer higher throughput, thereby further reducing delay and improving overall performance. Additionally, lightweight algorithms are introduced to adapt these parameters dynamically based on network conditions. The proposed model is validated through simulations, showing strong agreement with the analysis and confirming its practical effectiveness.</p>
25.	<p><a href="#"><u>Boger fluid droplet impact and interaction regimes on anti-wetting spheres</u></a>  <b>M Singh, M Tanyang, P Dhar, D Samanta - Physics of Fluids, 2025</b></p> <p><b>Abstract:</b> Droplet impact events on curved surfaces are commonly observed in both nature and man-made systems. It is anticipated that the curvature shall significantly affect the post-impact dynamics and regimes. This study explores the dynamic behavior of elastic fluid (Boger fluid) droplets impacting superhydrophobic spheres. In our experiments, we have highlighted the variations in the post-impact dynamics arising from the elastic properties of the fluid and the curvature of the surface. It was found that the secondary droplets, typically observed in the case of Newtonian fluids, transformed into enduring, slender filaments due to the fluid's elastic behavior. Depending on the polymer concentration (used to synthesize the Boger fluids), these filaments either disintegrated into secondary droplets or retracted to merge back into the parent droplet, which ultimately rebounded off the spheres. The rebound suppression phenomenon, observed and reported in elastic fluid droplets on flat superhydrophobic surfaces, does not take place on spherical surfaces due to the curvature effect. Subsequently, a regime map encompassing all the post-impact outcomes is presented as a function of the Weber number, and a non-dimensional parameter that captures the effect of droplet impact velocity, the relaxation time of the fluid, and the sphere diameter.</p>
26.	<p><a href="#"><u>Controlling Mg anode interface for achieving high-performance Mg-air batteries in seawater-based hybrid electrolyte</u></a>  <b>AP Sinha, TS Thomas, D Mandal - Journal of Power Sources, 2025</b></p> <p><b>Abstract:</b> Aqueous Mg-air batteries are potential candidates for next-generation energy storage devices owing to the usage of cost-effective Mg anodes, recyclability, high theoretical specific capacity, and abundant Mg reserves. The stability of Mg anode in neutral electrolytes renders seawater a viable electrolytic medium. However, severe corrosion and hydrogen evolution reaction (HER) hinder its practical application, resulting in poor anodic utilization and energy density. To overcome these issues, a hybrid electrolyte is developed comprising sodium acetate (NaOAc) and polyethylene glycol (PEG-400). The hybrid electrolyte is designed to protect the Mg substrate from aggressive chloride ions by enhancing the kosmotropic effect of acetate with PEG, while restricting the total additive content to 20 wt%. The Mg-air battery assembled by integrating NaOAc and PEG-400 with the seawater as the electrolyte medium exhibits an impressive lifetime of 298 h with a high energy density of 2001 Wh kg<sup>-1</sup> @1 mA cm<sup>-2</sup>, thereby demonstrating an excellent self-corrosion inhibition efficiency of the designed hybrid electrolyte, while utilizing cost-effective and abundant seawater. This work provides a practical and scalable solution for</p>

	<p>high-performance Mg-air batteries for commercially viable and sustainable use in energy storage applications.</p> 
27.	<p><a href="#">Defining the role of mobility as a service—A discrete choice framework incorporating missing data</a>  <b>TM Rahul, B Aaditya, Nikhil</b> - <i>Travel Behaviour and Society</i>, 2026</p> <p><b>Abstract:</b> Mobility as a Service (MaaS) is an emerging concept that integrates various sustainable and shared modes using a digital interface. Currently, it is promoted as an option that encourages shift from private vehicles. Its preference among private vehicle non-users is unexplored. The current study models the willingness of individuals to choose a MaaS package consisting of Mass Rapid Transit System (MRTS), bus and shared bicycle options in the city of Chandigarh, India using an Integrated Choice and Latent Variable (ICLV) framework. It addresses the issue of missing income, in the data collected, by assuming the income variable to be latent in the ICLV model. The structural and measurement equations of the latent income variable are specified using novel error formulations having either normal or lognormal distributions. Among the models estimated, multiplicative models with lognormal error distribution in the structural and measurement equations were observed to result in a better fit than the conventional model with normal error distributions in both structural and measurement equations. Across models, income and environmental consciousness were found to significantly increase the preference for MaaS. Further, our results highlighted a need for improving the quality of existing shared modes and public transport that are included in the MaaS subscription. The preference for MaaS among low-income respondents, and females, who do not have a driving license, indicated that MaaS can be considered as an option to address the issue of transportation inequity, especially for people having low chances of owning a private vehicle.</p>
28.	<p><a href="#">Demographic transition and financial assets</a>  <b>K Rai, B Garg</b> - <i>Emerging Markets Review</i>, 2025</p> <p><b>Abstract:</b> This study examines the impact of changing age structures on risky and risk-free assets. Considering that demographic transition is lagged in emerging market economies (EMEs) but the change in age structures will be more rapid than in advanced economies (AEs), we consider two panels of AEs and EMEs. Unlike previous literature on the demographic transition, we address the issue of cross-sectional dependence and slope heterogeneity. Our key findings suggest that the prime working-age population significantly influences both risky and risk-free assets in AEs and EMEs alike. However, the old-age dependency ratio tends to have a different impact on risk-free assets.</p>
29.	<p><a href="#">Differential representation for Carrollian correlators</a>  <b>S Chakraborty, S Hegde, A Maurya</b> - <i>Journal of High Energy Physics</i>, 2025</p> <p><b>Abstract:</b> The differential representation of AdS correlators offers a framework to express exchange Witten diagrams as functions of non-local differential operators applied to contact Witten diagrams. In this paper, we develop the differential representation for scalar Carrollian correlators. We first construct this representation using the recently formulated Carrollian limit of AdS Witten diagrams. We then provide an alternate intrinsic analysis that leverages the properties of the Carrollian bulk-to-boundary propagator. Using the differential representation, we also obtain differential Bern-Carrasco-Johansson (BCJ) relations for Carrollian correlators.</p>
30.	<p><a href="#">Dynamic properties of jointed rocks under diverse loading conditions: Insights from experimental and predictive modelling</a>  <b>S Rohilla, R Sebastian, A Bhamidipati</b> - <i>Tunnelling and Underground Space Technology</i>, 2025</p>

**Abstract:** Discontinuities such as joints play a pivotal role in defining the dynamic response of rock masses. While joint roughness and orientation are known to influence wave propagation and energy dissipation, there exists a lack of comprehensive experimental studies that quantify their combined effects under varying loading conditions. This study addresses this gap by systematically investigating the influence of joint properties and dynamic loading parameters on the shear modulus, damping ratio, and resilient modulus of jointed rocks. Gypsum plaster specimens were prepared with controlled joint roughness coefficients ( $JRC = 6-8, 12-14, \text{ and } 18-20$ ) and orientations ( $30^\circ, 45^\circ, \text{ and } 60^\circ$  from the horizontal plane) using 3D-printed moulds. Dynamic properties were evaluated under a range of strain amplitudes ( $0.0001\% - 0.1\%$ ), confining pressures ( $50-2500 \text{ kPa}$ ), and loading frequencies ( $0.1-10 \text{ Hz}$ ) using resonant column and cyclic torsional shear tests. The results revealed that increasing joint roughness and orientation generally led to higher shear modulus and lower damping ratios at small strain levels. However, under higher confining pressure and strain amplitudes, joint degradation caused by asperity breakdown reduced stiffness and increased damping, indicating a complex interplay between loading and joint characteristics. To predict dynamic behaviour, both multiple linear regression and Random Forest (RF) models were employed. While linear regression captured basic trends, RF outperformed it with a  $15-20\%$  improvement in coefficient of determination ( $R^2$ ) and a significant reduction in root mean square error (RMSE), effectively modelling the nonlinear relationships between variables. Although the study focuses on shear modulus and damping ratio, it also presents a method to estimate the resilient modulus of jointed rocks under varied dynamic conditions, offering broader engineering applicability. These findings contribute toward developing predictive tools for dynamic rock analysis and have direct implications for tunnelling, mining, and vibration-sensitive infrastructure design.

[Effect of salinity on root water uptake in paddy and wheat: A comparative study and parameter estimation](#)

G Goet, I Sonkar, KS Hari Prasad... - Journal of Irrigation and Drainage Engineering, 2025

31.

**Abstract:** Soil salinity poses a significant challenge to agricultural productivity, especially in arid and semiarid regions, where the accumulation of excessive salts in the root zone impedes water uptake and adversely affects crop growth. A comprehensive understanding of the effects of salinity on root water uptake is essential for developing optimized irrigation practices and promoting sustainable crop production. This research investigates the effect of varying salinity levels on the root water uptake (RWU) pattern using nonlinear Ojha and Rai RWU model. Experiments were conducted at six salinity levels ( $0.5, 5, 10, 15, 20, \text{ and } 25 \text{ dS/m}$ ), on paddy (*Oryza sativa L.*) and wheat (*Triticum aestivum*), within a controlled experimental environment. The optimization algorithm was tested using synthetically generated soil moisture data, demonstrating a strong agreement with the actual values which confirms the efficacy of the model. The results indicate decrease in nonlinear RWU pattern parameter  $\beta$  and the root depth, with increase in salinity levels. The  $\beta$  parameter varies from 1.953 to 1.825 for paddy and from 1.543 to 1.348 for wheat at salinity levels of  $0.5 \text{ dS/m}$  and  $25 \text{ dS/m}$ , respectively. Root depth for paddy decreases by  $35.98\%$  and  $51.47\%$  for wheat crop, comparing minimum and maximum salinity levels. The simulated moisture profiles using the optimized  $\beta$  values are in strong agreement with the field-observed soil moisture content across the different layers in the root zone. Moreover, irrigation with highly saline water ( $25 \text{ dS/m}$ ) resulted in an approximate reduction of  $81\%$  in peak RWU recorded for paddy and  $56\%$  for wheat, compared to irrigation with low salinity water ( $0.5 \text{ dS/m}$ ). The coefficient of determination ( $R^2$ ) and Nash Sutcliffe efficiency ( $NSE$ ) values for soil moisture variation across different salinity levels range from  $0.887$  to  $0.941$  and  $0.846$  to  $0.908$  for paddy and  $0.872$  to  $0.955$  and  $0.828$  to  $0.913$  for wheat respectively, indicating the efficacy of the model even under high salinity stress. As a result of higher osmotic stress, the soil moisture depletion decreases for both crops with the elevating salinity levels. This study advances the application of the nonlinear Ojha and Rai RWU model by incorporating an optimization-based approach to estimate the nonlinearity parameter ( $\beta$ ), improving its applicability in saline-irrigated conditions. Additionally,

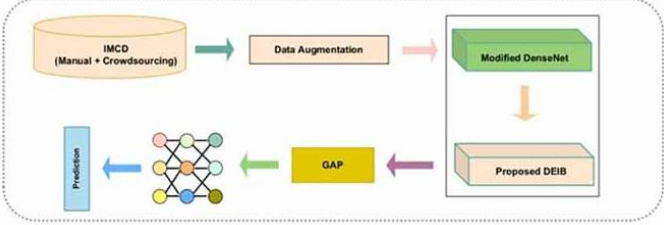
	<p>a comparative analysis of paddy and wheat under varying salinity levels provides new insights into crop-specific responses, establishing its usefulness in salinity-affected irrigation systems.</p>
32.	<p><a href="#">Efficient and sustainable closed-loop recycling of broad range polyester plastic wastes over in situ grown bifunctional ZnO–SiO<sub>2</sub> catalysts</a>  <b>AK Manal, A Gupta, R Srivastava - Advanced Sustainable Systems, 2025</b></p> <p><b>Abstract:</b> The growing accumulation of plastic waste presents serious environmental and health concerns, necessitating efficient recycling technologies to support a circular economy. Here, a cost-effective and efficient catalyst is reported for depolymerizing polyethylene terephthalate (PET) and various polyesters into their respective monomers. This closed-loop recycling strategy is inspired by solvolysis and enabled by a bifunctional acid–base ZnO–SiO<sub>2</sub> catalyst. An in situ growth method enhances metal–support interactions at the Zn–O–Si interface, leading to the formation of Zn–O–Si species and well-dispersed small ZnO nanoclusters (≈3.5 nm), which generate abundant acid–base active sites. The optimized catalyst achieved a 94% yield of bis(2-hydroxyethyl) terephthalate (BHET) from PET glycolysis at 180 °C in 1.5 h under co-solvent-free conditions. It further exhibits high catalytic efficiency in the methanolysis of PET and other polyesters (polybutylene terephthalate (PBT), polybutylene succinate (PBS), and polylactic acid (PLA)), with monomer yields above 90%. A scale-up experiment with 10 g PET delivers ≈90% BHET yield, confirming the catalyst's practical applicability. Green chemistry metrics are used to validate the efficiency and sustainability of the process. The high monomer productivity (40–50 g<sub>monomer</sub>·g<sub>catalyst</sub><sup>-1</sup>·h<sup>-1</sup>) and reduced environmental footprint highlight the promise of this system for sustainable plastic upcycling.</p> <p>Graphical Abstract</p> <p><small>Although global efforts toward plastic waste recycling are increasing, sustainable and cost-effective catalytic protocols for the efficient depolymerization of a broad range of polyesters remain scarce. Here, this study reports an in situ growth strategy that enhances Zn–O–Si interfacial interactions and generates well-dispersed ZnO nanoclusters providing abundant acid–base sites for selective monomer recovery (&gt;90% yields) under mild conditions.</small></p> 
33.	<p><a href="#">Emerging role of aqueous batteries in next generation energy-dense sustainable storage</a>  <b>AP Sinha, TS Thomas, D Mandal - Chemical Communications, 2025</b></p> <p><b>Abstract:</b> Aqueous metal batteries are emerging as promising candidates for next-generation energy storage, offering safer, more sustainable, and cost-effective alternatives to lithium-ion batteries (LIBs). Leveraging earth-abundant metals such as zinc, aluminium, magnesium, and silicon, these systems benefit from non-flammable, water-based electrolytes and simplified manufacturing, making them attractive for grid-scale and off-grid applications. This review highlights recent progress in aqueous battery chemistries, including metal-ion, metal-sulfur, and metal-air systems, emphasizing advancements in electrode design, electrolyte engineering, and interface optimization to improve energy density and cycling stability. Key challenges such as dendrite formation, self-corrosion, and parasitic reactions are critically examined, along with emerging solutions like functional additives, protective coatings, and nanostructured materials. This review underscores the potential of aqueous batteries in supporting decarbonized energy infrastructures by categorizing systems according to charge-storage mechanisms and life cycle assessment (LCA) indicators. Although unlikely a universal replacement for LIBs, aqueous systems offer highly viable solutions for stationary storage, requiring further research, scalable design strategies, and targeted investment to transition from laboratory innovation to commercial deployment. Finally, this review discussed the trade-off between various aq. battery systems and concludes with key research priorities and policy recommendations to guide future development aligned with LCA principles.</p>
34.	<p><a href="#">Engineering aesthetics generic definition, tests, factors, and methods</a>  <b>J Singh, P Sarkar - International Journal of Design Creativity and Innovation, 2025</b></p>



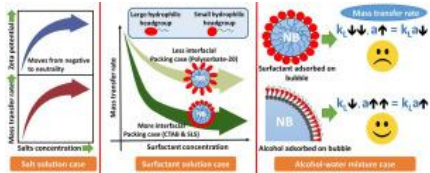
	<p><b>Abstract:</b> In recent times, aesthetics has been one of the most critical factors during the product development phase influencing the success of many organizations. However, many factors, measurement ways, and methods for aesthetics make it challenging for industries to consider an appropriate measurement way, constituents feature, and method for providing support/help for enchaining the product's aesthetics. In this work, we first synthesize a standard definition of aesthetics in philosophy, proposed by different authors in various literature. Using this definition, we identify the core constituents or features which were related to the aesthetics in engineering and develop an engineering aesthetics definition. This study can help in identifying, understanding, and quantifying the engineering aesthetics definition. Using this description, we define engineering aesthetics metrics that could be used to evaluate human aesthetics, factors influencing aesthetics, and techniques for improving aesthetics. This study demonstrates that a corporation can choose a particular set of tests and techniques based on how much attention is paid to the key engineering aesthetics characteristics that are derived from the common definition.</p>
35.	<p><a href="#"><u>Enhancing building roof thermal energy efficiency in hot climates: A novel dual-layer design with integrated phase change materials</u></a>  <b>AB Huluka, S Muthulingam - Energy and Buildings, 2025</b></p> <p><b>Abstract:</b> In hot climates, space cooling in buildings is essential due to high temperatures and solar radiation, which increase indoor heat gain and energy consumption. Roofs, as primary building envelopes, contribute significantly to this heat transfer. Phase change materials (PCMs) enhance thermal mass and reduce heat transfer, yet large-scale PCM integration strategies in roofs for effective thermal management in hot climates remain largely unknown. The present study proposes a novel dual-layer PCM integrated roof for enhanced thermal performance in hot climates. First, PCM was selected, characterized, and macroencapsulated, then embedded in a concrete matrix to form the first layer. Second, a hollow clay tile (HCT) was designed, manufactured, characterized, and integrated with or without PCM to create the second layer. Following the sector approach, which allowed testing of more variables, the dual-layer was divided into four sectors: Sector 1 (S-1) with conventional concrete and HCT modules; Sector 2 (S-2) with empty capsules and HCT modules; Sectors 3 (S-3) with PCM capsules and HCT modules; and Sector 4 (S-4) with PCM capsules and PCM-HCT modules. The thermal performance of this dual-layer roof exposed to ambient conditions was then evaluated by analyzing various latent heat storage parameters, such as temperature profiles, thermal performance index, thermal damping, heat flux variations, heat gain, thermal load leveling, decrement factor and CO2 emission savings. Average indoor temperature reductions were 10.9 °C in S-1, 16.5 °C in S-2, 16.6 °C in S-3, and 17.3 °C in S-4. S-3 and S-4 showed the best thermal regulation with the lowest performance index, 80 % heat flux reduction, 75 % heat gain reduction, high efficiency, and the lowest thermal load leveling. This study offered valuable insights for designing dual-layer roofs to improve indoor thermal regulation in hot climates.</p>
36.	<p><a href="#"><u>Eternal connected vertex cover problem in graphs: Complexity and algorithms</u></a>  <b>K Paul, A Pandey - Theoretical Computer Science, 2025</b></p> <p><b>Abstract:</b> This paper deals with a dynamic variant of vertex cover problem, known as the eternal vertex cover problem. This is a two-player (attacker and defender) game, where the defender must allocate guards at specific vertices in order for those vertices to form a vertex cover. The attacker can attack one edge at a time. To defend the attack, the defender must move the guards along the edges so that at least one guard moves through the attacked edge (the guard moves from one end point of the attacked edge to the other end point), and the new configuration still acts as a vertex cover. If the defender can not make such a maneuver, the attacker prevails. If the defender can defend the graph against any infinite sequence of attacks, then the defender wins, and we say the defender can defend the graph. The eternal vertex cover problem is to find the smallest number of guards with which the defender can defend the graph. The same problem is referred to as the eternal connected vertex cover problem if the following additional condition is added: underlying</p>

	<p>vertices of each defensive configuration form a connected vertex cover. The smallest number of guards that can be used to create a successful defensive strategy, in this case, is known as the eternal connected vertex cover number and is denoted by the <math>ecvc(G)</math>. The decision version of the eternal connected vertex cover problem is NP-hard for general graphs and remains NP-hard even for bipartite graphs. In this paper, we propose polynomial time algorithms to find the eternal connected vertex cover number in chain graphs, cographs and certain kinds of bipartite graphs. An efficient algorithm to compute connected vertex cover number for Mycielskian of a Hamiltonian graph <math>G</math> (for which the Hamiltonian cycle is also given as part of the input) is also proposed in this paper. In addition, minimum vertex cover number and eternal connected vertex cover number are also computed for the same graphs. Further, We show the existence of a linear time algorithm to solve the minimum connected vertex cover problem for distance-hereditary graphs.</p>
37.	<p><a href="#">F18 promiscuous epitope of Acr1 protein of mycobacterium tuberculosis induces the secretion of IL-10 and Tregs but not IL-6</a>  <b>T Lamba, S Prajapati, A Chowdhury, A Bandyopadhyay, JN Agrewala - Protein and peptide letters, 2025</b></p> <p><b>Abstract:</b> Introduction: Mycobacterium tuberculosis (Mtb) is a Gram-positive bacterium that causes tuberculosis (TB). It remains viable for extended periods within host macrophages by entering a dormant state. Alpha crystallin 1 (Acr1) is a 16 kDa protein of Mtb and is reported to be highly upregulated in latent TB. Acr1 suppresses the host's immune system by impairing the differentiation and maturation of dendritic cells and macrophages. We hypothesize that Mtb judiciously utilizes its Acr1 protein to paralyse the immune system of the host by inducing the release of IL-10 and generating an immunosuppressive environment. Methods: We employed in silico tools to identify highly promiscuous, IL-10-inducing and IL-6- non-inducing epitopes of Mtb. Moreover, the selected epitope was synthesized and tested for its suppressive activity and generation of Tregs. Results: We identified the presence of a specific epitope in Acr1 (F18) that is responsible for bolstering the release of IL-10 and Tregs through in silico tools and verified the activity by in vitro assays. In hPBMCs, the F18 epitope could suppress the proliferation of CD4 T cells stimulated with PHA and expand the pool of Tregs in a dose-dependent manner. Discussion: The F18 epitope from Mtb's Acr1 protein promotes IL-10 and Treg responses without triggering pro-inflammatory IL-6, suggesting a potential immunoregulatory role. While it holds potential for treating autoimmune diseases, its impact on infection tolerance in tuberculosis should be further investigated. Conclusion: Our findings suggest that the F18 epitope induces IL-10 production and Treg differentiation while inhibiting CD4+ T cell proliferation and IL-6 secretion, thereby promoting an immunosuppressive environment. Furthermore, this study highlights the potential of Acr1 and its immunosuppressive epitope F18 as therapeutic agents for inducing suppressive Tregs in the management of autoimmune diseases.</p>
38.	<p><a href="#">Graphic journeys: Virtual dark tourism in Joe Sacco's Palestine and Footnotes in Gaza</a>  <b>N Soman, KS Swathi - Visual Studies, 2025</b></p> <p><b>Abstract:</b> The article examines how Joe Sacco's war comics Palestine (1993) and Footnotes in Gaza (2009) engender virtual dark tourism experience for its readers through the Occupied Territories using the unique possibilities of the graphic medium such as sequential arrangement of panels, cartographic representation, sonic effects, focalization, shifting perspectives, and recurring visual motifs, among others. Espousing the identity of a Western tourist in search of stories of collective suffering and depravity, Sacco navigates the refugee settlements of West Bank and Gaza Strip to illustrate the anxious everyday existence of Palestinian residents, which is often disregarded by mainstream media narratives. Appropriating the multimodality and visual language of the comics medium, Joe Sacco, this paper argues, turns his readers into fellow dark tourists on his journeys across the contested lands of West Asia in order to witness and experience the woes of the marginalized and oft misrepresented Palestinians under occupation. Furthermore, the study underscores how the graphic medium can be a potent tool to emulate the experientiality of a dark tour.</p>

39.	<p><a href="#">Growing up in the “Dirty South”: Precarious black childhoods in Jesmyn Ward's <i>Sing, Unburied, Sing and Salvage the Bones</i></a>  <a href="#">S Reji, A Nandha - The Black Scholar, 2025</a></p> <p><b>Introduction:</b> Christina Sharpe’s <i>In the Wake: On Blackness and Being</i> (2016) deliberates how “literature, performance, and visual culture observe and mediate” the “ontological negation” 1 of Black lives. Contemporary writer Jesmyn Ward’s canon harbors an answer to Sharpe’s inquiry, for her narration of the Dirty South contextualizes the dehumanization of Black people in the twenty-first-century United States of America. She portrays the ethos of ordinary Southern rural life by rendering the violent relationship among structures of inequality, haunted landscapes and the dispossessed Black community in the South. By echoing the legacy of Southern writers yet simultaneously rejecting “stagnant notions” 2 of the earlier representations, Ward delineates predominant themes such as racism, childhood, trauma, poverty, and everyday precarity. She reconstructs the traditional tropes of the coming-of-age narrative, the gothic and the road narrative to amalgamate mundane African American experiences and therefore her works inevitably garner international attention. Her agenda of unapologetically engaging with the politics of representation dates back to her experiences of growing up as a Black child who “starved for fictional representation.” 3 She reflects that, even as a writer, she required considerable time to unlearn the misrepresentation “and to reach a point where I [Ward] can confidently say that our [Black] lives are just as human and complicated and fascinating as anyone else’s.” 4 Maintaining this position, her corpus offers a nuanced portrayal of Black people, effortlessly evading the debates on stereotypes and instead portraying the “rawness” of their lives with “honesty.” 5 Her narratives detail the struggles of marginalized Black people negotiating their everyday lives in Bois Sauvage, a fictional place modeled on her hometown DeLisle. Ward integrates the elements of the Dirty South to represent her community that has been historically “devalued” and labeled “nugatory.” 6 Dirty South emerged as a subgenre of hip hop, marketing the regional and racial identity of the South. 7 Translating its essence, Ward investigates the regional identity, repressed voices and historical silences by narrativizing the mundane experiences of the Southerners. Her young protagonists live in the Pit, a deserted piece of land deep inside Bois, where they gather for fierce dog fights or a swim by the dirty lake. By portraying children thriving in ghettoized neighborhoods she chronicles their perseverance in constructing alternate social structures in the absence of a nurturing environment. Drawing from Patricia Yaeger’s foundational study <i>Dirt and Desire</i> (2000) that contextualizes Southern women writers, critic James Crank writes about notions that are typically attributed to the South by public imagination, like “the dirty, the shameful, the repressed, the forgotten, the damaged, the underrepresented, [and] the trash.” 8 Reinforcing Crank’s claim, the overarching themes of Ward’s canon on the South’s dirt 9 “with a courage born of desperation.”</p>
40.	<p><a href="#">ICDRF: Indian coin denomination recognition framework</a>  <a href="#">MS Kanroo, HS Kawoosa, K Rana, P Goyal - IEEE Access, 2025</a></p> <p><b>Abstract:</b> Coins are commonly used in everyday transactions at supermarkets, retail shops, metro stations, and other locations. However, recognizing Indian coin denominations poses a challenge for visually impaired persons due to the lack of a robust coin denomination recognition system. To address this issue, we introduce the Indian Coin Denomination Recognition Network (ICDRNet), a deep convolutional neural network (CNN) tailored for the visual recognition of Indian coin denominations. ICDRNet combines densely connected convolutional layers with depthwise separable dense blocks, incorporating the Convolutional Block Attention Module (CBAM) and a novel Dilation Enabled Inverse Bottleneck (DEIB) block. The integration of CBAM enhances the model’s ability to highlight critical features across different coins by prioritizing essential spatial and channel information, thereby improving recognition accuracy. The DEIB block employs dilated convolutions to efficiently capture detailed features across various scales, focusing on subtle distinctions among coin denominations with minimal computational overhead. Furthermore, we present the Indian Metal Currency Dataset, a comprehensive collection of images representing Indian coins under diverse lighting, background,</p>

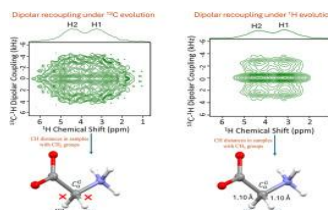
	<p>and environmental conditions, facilitating a robust evaluation of coin recognition performance in realistic scenarios. Experimental results show that the proposed method shows improved performance in identifying coin denominations compared to prior methods on the proposed Indian Metal Currency Dataset (IMCD), Indian Coin Currency Dataset (ICCD), Indian Coin Denomination Dataset (ICDD) &amp; Comprehensive Image Dataset of Contemporary Indian Coins (CIDCIC) datasets. ICDRNet achieves an impressive performance with F1-score of 97.79%, 98.38%, 96.7% and 99.7% on IMCD, ICCD, ICDD &amp; CIDCIC datasets, respectively.</p> 
41.	<p><a href="#">Identifying efficient policy mix under emission mitigation and inflation targeting: A case of India</a>  <b>SA Shah, B Garg, P Sahoo - Energy Economics, 2025</b></p> <p><b>Abstract-</b> This article investigates the business cycle dynamics of different environmental policy interventions, to offer a viable solution for balanced macroeconomic stability with effective emission reduction. From the New Keynesian macroeconomic analysis, our findings imply a leading role of cap and trade policy in abating excessive emissions with a favorable macroeconomic effect. Of note, the results also indicate the significant role of inflationary targeting monetary policy relative to the conventional monetary policy in controlling the rising carbon emission. Our analysis passes several robustness checks. Overall, findings imply that the cap and trade policy, if operated under the inflationary targeting monetary policy framework, will result in a more efficient outcome as it not only increases output and reduces emissions but also controls the escalating inflation. However, the unrestricted use of this policy intervention for emission mitigation may be ill-advised because it can contribute to regional emission asymmetry.</p>
42.	<p><a href="#">Instability onset and energy growth in two-layer miscible channel flows: Insights via initial value problem</a>  <b>P Banga, SN Maharana, M Mishra - Physical Review Fluids, 2025</b></p> <p><b>Abstract:</b> This study investigates the linear stability of viscosity-stratified miscible two-layer flows in a channel, addressing the inherent complexity introduced by the time-dependent base state resulting from diffusion of solute concentration at the interface. Unlike previous studies that rely on the quasi-steady-state approximation (QSSA), which neglects the transient nature of the base state by assuming it remains frozen, we employ an initial value problem (IVP) approach to incorporate the unsteady base state into the stability analysis. Employing the IVP approach, we solve the linearized incompressible Navier-Stokes and convection-diffusion equations. We demonstrate that, unlike QSSA, the IVP method effectively provides critical insights into early-time perturbation growth, primarily driven by initial diffusion, and accurately predicts the onset time of instability. Through energy amplification analysis, we compute perturbation growth rates over time, revealing their nonmonotonic dependence on the log-mobility ratio (<math>R</math>) and mean interface location (<math>h'</math>). We show that the growth rates increase monotonically with increasing Reynolds (<math>Re</math>) and Péclet (<math>Pe</math>) numbers, and decrease with increasing interface thickness (<math>\delta</math>). Systematic analyses further unveil a nonmonotonic dependence of onset time of instability (<math>t_{on}</math>) on <math>R</math>, identifying critical values of the log-mobility ratio for instability onset. These critical values, <math>R_{cl}</math> and <math>R_{cu}</math>, are influenced by <math>Re</math>, <math>Pe</math>, <math>h'</math>, and <math>\delta</math>. Through an energy budget analysis of concentration perturbations, we highlighted the interplay between convection and diffusion in determining the overall perturbation growth rates, thereby explaining the observed nonmonotonic variation with the log-mobility ratio <math>R</math>.</p>
43.	<p><a href="#">Interfacial engineering of nanobubbles: From nucleation to mass transfer</a>  <b>H Sharma, G Yadav, N Dutta, N Nirmalkar - Surfaces and Interfaces, 2025</b></p>



	<p><b>Abstract:</b> Nanobubbles (NBs) have a sub-micron size and a large specific surface area, making them promising agents for improving gas–liquid mass transfer rates. Their effectiveness is directly associated with their stability, interfacial behavior, and response to physicochemical conditions, including surface activity and ionic strength. This study systematically investigates the generation and behavior of oxygen nanobubbles (ONBs) utilizing a nanopore gas diffusion technique across three separate categories of aqueous environments: surfactants, salts, and alcohol–water mixtures. At the same time, the evaluation of gas–liquid mass transfer performance is performed by analyzing dissolved oxygen (DO) versus time profiles and measuring volumetric mass transfer coefficients (<math>k_{LA}</math>). The findings indicate that although surfactants and alcohols in water facilitate the formation of NBs through the reduction of surface tension, their impacts on the <math>k_{LA}</math> differ significantly. The addition of alcohols in water results in increased NB concentrations and an enhanced <math>k_{LA}</math>. In contrast, surfactants also yield higher NB concentrations and stabilize NBs; however, they decrease <math>k_{LA}</math> due to increased interfacial resistance to gas diffusion. Salts enhance <math>k_{LA}</math> by accelerating the generation and collapse of NBs, even though they reduce the stability of NBs due to electric double layer (EDL) screening. The findings are correlated with a nanopore-based theoretical model that predicts the minimum bubble pinch-off radius (<math>R</math>) as a function of surface charge and surface tension. The study provides an in-depth analysis of the influence of EDL modulation and interfacial adsorption on the formation and utilization of NBs in gas–liquid mass transfer systems.</p> 
44.	<p><a href="#">Interplay of electronic and magnetic phase modulation in a spin-polarised nanomagnet</a>  S Kar, N Gupta, D Roy, SJ Ray - Scientific Reports, 2025</p> <p><b>Abstract:</b> The 2H-phase of monolayer vanadium diselenide (VSe) has recently emerged as a very intriguing material in spintronics due to its intrinsic ferromagnetism with semiconducting properties. In the present work, first-principles based calculations have been employed to systematically study the electronic, magnetic, and optical behaviour of 2D VSe for investigating the impact of different external excitations such as strain, electric field, and pressure on the material. Specifically, the magnetic moment, band gap, Curie temperature (<math>T</math>), and absorption coefficient could be modulated, as the states near the Fermi level are mainly contributed by the in-plane atomic orbitals. The presence of different electronic phases in 2D VSe can be modulated from semiconductor to half-metal and even normal metal under the influence of external stimuli. Furthermore, the in-plane biaxial strain can effectively tune the <math>T</math> and attains a maximum value of 354K at = 6%. The maximum observed absorption coefficient is found to be 5.05 10 cm (at 1.4 eV) under the applied pressure of 30 GPa, indicating that the VSe exhibits strong light absorption in the visible region. The unique combination of electronic phases, robust ferromagnetism, and optical activity makes the 2H-VSe a suitable candidate for flexible electronic, optoelectronic, and spintronic applications.</p>
45.	<p><a href="#">Investigation of a novel symmetric-structure based mems piezoresistive accelerometer</a>  S Singh, V Kumar, N Kumar - IEEE Transactions on Components, Packaging and Manufacturing Technology, 2025</p>

	<p><b>Abstract:</b> In this paper, a novel symmetric-structure-based silicon MEMS (Micro Electro Mechanical Systems) piezoresistive accelerometer is proposed. Compared to conventional structures based on multiple support beams and hanging seismic mass, the symmetric-structure not only reduces cross-axis output but also ensures lower stresses in the flexures when subjected to cross-axis acceleration inputs. It increases the fracture acceleration limit in the cross direction, relative to the sensing direction, from approximately 5.8 to 24 times. Additionally, it improves the ratio of the second to the first mode frequency from 1.6 to 10, which improves survivability of the structure over a much wider bandwidth against resonance of the second mode. The new structure was fabricated by bonding two SOI (Silicon-on-Insulator) wafers, each containing complementary halves of the structure. This paper presents the configuration details of the structure, along with analytical and FEA (Finite Element Analysis) results to estimate deflections, stresses, modal frequencies, and mode shapes. Additionally, the MEMS fabrication process details, packaging, and test results of X-ray imaging, SEM (Scanning Electron Microscope) imaging, natural frequency measurement using LDV (Laser Doppler Vibrometer), sensitivity test, and so on, at die and package level are discussed.</p>
46.	<p><a href="#">Manufacturing of Ti6Al4V alloy using argon chamber assisted WAAM-CMT to avoid oxidation and analyses of mechanical and metallurgical properties</a>  J Singla, N Kumar, A Bansal - Journal of Alloys and Compounds, 2025</p> <p><b>Abstract:</b> Titanium alloy, namely Ti6Al4V, has been extensively employed for the development of lightweight and high-strength components in industries like aerospace, automobile, and biomedical equipment. Direct energy deposition (DED) techniques under the umbrella of additive manufacturing (AM) are highly acclaimed for the manufacturing of complex components. Among different AM techniques, Wire Arc Additive Manufacturing-Cold Metal Transfer (WAAM-CMT) has emerged drastically owing to properties like the ability to create larger components, high deposition rate, low material wastage, and cost. However, the problem of oxidation during the development of Ti6Al4V alloy is very critical, and the same has to be mitigated for better performance of the alloy. Therefore, in this research work, in the 1st phase, an anti-oxidation chamber was designed and built to provide total Argon shielding as and when desired. Further, in the 2nd phase, a Ti6Al4V block with one portion in argon and another portion without an argon atmosphere was developed utilizing the WAAM-CMT technique and analyzed for various metallurgical and mechanical properties. Argon shielding was found to be effective in providing resistance to oxidation. It showed a defect-free layer interface with microstructural features of fine and coarse basket weave, along with higher fractions of high-angle grain boundary and low KAM, with the absence of oxide phases like TiO<sub>2</sub> and Al<sub>2</sub>O<sub>3</sub>. However, for alloys developed in the open air, due to the development of a hard and brittle oxidized interlayer, the microhardness was found to be highest at the layer intersection. Due to repeated thermal cycles for the bottom bead, microhardness was found to be higher than that of the top bead. Argon shielding also provides better tensile strength and toughness, with longitudinal orientation standing out as best, owing to intra-layer failure. Argon shielded specimen underwent ductile mode of failure with mechanistic features of well-formed dimples; however, for alloy developed in open air, due to the presence of hard and brittle oxidized interlayer, traces of brittle dust along dimples were reported, which justifies a mixed (ductile and brittle) mode of fracture.</p>
47.	<p><a href="#">Measurement of C–H distances in solids at natural abundance via proton-detected fast MAS NMR spectroscopy</a>  Y Bhardwaj, KK Rohilla, Y Nishiyama, MK Pandey - Solid State Nuclear Magnetic Resonance, 2025</p> <p><b>Abstract:</b> Measurement of heteronuclear distances from the radio-frequency (rf) pulse-based recoupling of NMR experiments is vital for structural refinement and dynamics studies at the atomic level. Despite advancements in the design and development of recoupling methods, the extraction of the directly-bonded heteronuclear XH distances in samples with XH<sub>2</sub> moieties remains challenging. This is primarily due to the interference effects from the neighboring</p>

spins/local fields leading to distorted dipolar coupling powder lineshapes. In this regard, we present a proton-detected 3D  $^{13}\text{C}$  chemical shift (CS)/ $^{13}\text{C}$ - $^1\text{H}$  dipolar coupling/ $^1\text{H}$  chemical shift (CS) correlation experiment under fast magic angle spinning (MAS), which has the potential to measure the directly-bonded CH distances in naturally abundant samples with  $\text{CH}_2$  groups. We have implemented the windowless ROCSA-based  $^{13}\text{C}$ - $^1\text{H}$  dipolar interaction recoupling scheme under  $^1\text{H}$  evolution to achieve undistorted  $^{13}\text{C}$ - $^1\text{H}$  dipolar coupling powder lineshapes in contrast to our previously reported windowless ROCSA-DIPSHIFT method under X-nuclei evolution, wherein extraction of the directly-bonded CH distances in samples with  $\text{CH}_2$  groups is shown to be sensitive to the presence of the local fields due to neighboring spins.  $^{13}\text{C}$ - $^1\text{H}$  distances reported from the method presented in this work are also validated from the results emerging from the quantum chemical calculations.



[Mobile agents on chordal graphs: Maximum independent set and beyond](#)  
**T Kaur, K Paul, K Mondal - Theoretical Computer Science, 2025**

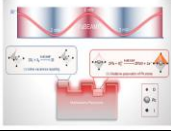
48.

**Abstract:** We consider the problem of finding Maximum Independent Set (MaxIS) for chordal graphs using mobile agents. Suppose  $n$  agents are initially placed arbitrarily on the nodes of an  $n$ -node chordal graph  $G=(V,E)$ . Agents need to find a Maximum Independent Set  $M$  of  $G$  such that each node of  $M$  is occupied by at least one agent. Also, each of the  $n$  agents must know whether its occupied node is a part of  $M$  or not. We provide distributed algorithms for  $n$  mobile agents, each having  $O(\log_{\tau_0} n)$  memory, to compute MaxIS of  $G$  in  $O(mn \log_{\tau_0} \Delta)$  time, where  $m$  denotes the number of edges in  $G$ ,  $n$  denotes the number of nodes in  $G$ , and  $\Delta$  is the maximum degree of the graph. At first, we design an algorithm considering the case where all agents are initially placed at the same node (i.e., rooted initial configuration). To run this algorithm, the agents do not require prior knowledge of any global parameter. Then we propose an algorithm for the case where agents are initially distributed arbitrarily across the graph (i.e., arbitrary initial configuration). To run this algorithm, the agents require prior knowledge of certain global parameters. Further, we provide faster algorithms for finding MaxIS in chordal graphs either by increasing the memory available to each agent or by employing more agents. We report that by using a similar approach, it is possible to find the maximum clique in chordal graphs and color any chordal graph with the minimum number of colors. We also provide a dynamic programming-based distributed algorithm to find a Maximum Independent Set for trees in  $O(n)$  time.

[Multifunctional passivation of Pb/I defect sites and carrier dynamics optimization based on femtosecond laser beat effect](#)  
**Z Huang... SR Konda, T Zou... - Laser & Photonics Reviews, 2025**

49.

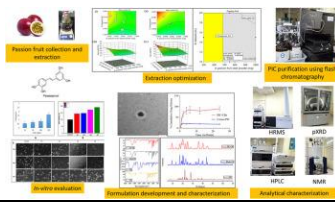
**Abstract:** As promising optoelectronic materials, lead halide perovskites (LHP) have been widely studied for their outstanding optoelectronic properties. However, the formation of halide vacancies ( $V_X$ ) and uncoordinated metallic lead atoms ( $\text{Pb}^0$ ) by ion migration, and consequent instability and nonradiative complexation, hinders their practical applications. Here, a femtosecond laser beat effect-assisted multifunctional passivation (FsBEAMP) approach is proposed to address these issues. Utilizing the beat effect of femtosecond laser pulses, a multifunctional passivation is achieved, which passivated the iodine vacancies ( $V_I$ ) and  $\text{Pb}^0$  simultaneously. For the FsBEAMP-processed samples, the hysteresis effect has been greatly reduced due to suppression of iodide ions migration. The 3-fold increase in PL intensity and 7-fold prolongation of carrier lifetime have been achieved due to multifunctional passivation effect and enhanced absorption caused by the periodic structure, allowing enhanced light-coupling effect. As a result, a 4-fold enhancement in responsivity and external quantum efficiency, along with a robust detectivity of  $2.5 \times 10^{12}$  Jones, has been realized for the FsBEAMP-processed photodetector. It is noted that the detectivity

	<p>remains 97% after a month in an ambient environment. This work will significantly contribute to the perovskite photonics and optoelectronics by providing a highly efficient way for multifunctional passivation of LHP.</p> <p style="text-align: center;">Graphical Abstract</p> <p style="text-align: center;"><small>Defect passivation is crucial for perovskite optoelectronic devices. Here, ferroelectric laser field effect-assisted multifunctional passivation (FSEAMP) is proposed to suppress iodine vacancies and uncoordinated Pb in MAPbI<sub>3</sub>. The chopper-induced periodic optical field increases iodine vacancy formation energy and promotes Pb-I bonds. Theoretical calculations show that FSEAMP significantly increases the formation energy and promotes Pb-I bonds, enhancing both photoluminescence and photoreponse performance.</small></p> 
50.	<p><a href="#">Noble-metal-free Cu(I)-catalyzed sp and sp<sup>2</sup> C–H carboxylation to produce high-value Compounds via CO<sub>2</sub> fixation under atmospheric conditions</a>  <b>PK Giri, P Rani, M Kaur, P Beniwal, TJ Dhillip Kumar, CM Nagaraja - ACS Applied Materials &amp; Interfaces, 2025</b></p> <p><b>Abstract:</b> The rise in anthropogenic carbon dioxide (CO<sub>2</sub>) emissions has significantly accelerated global environmental degradation, necessitating controlled measures to achieve carbon neutrality by utilizing CO<sub>2</sub> as a C1 feedstock for the preparation of important commodity products and fuels. Herein, we demonstrate the rational design and preparation of a precious metal-free catalyst (Cu(I)@Zr-MOF) by anchoring Cu(I) ions to functionalized Zr-MOF. Notably, Cu(I)@Zr-MOF exhibited high selectivity for CO<sub>2</sub> uptake with a surface area of 1083 m<sup>2</sup>/g. The high concentration of catalytically active Cu(I) sites present in the 1D channels of Cu(I)@Zr-MOF facilitated the efficient transformation of CO<sub>2</sub> into phenylpropionic acids via the carboxylation of C(sp)-H bonds under mild conditions. Additionally, Cu(I)@Zr-MOF enabled the carboxylation of heterocyclic precursors, such as 4-hydroxy-2-pyridones, with CO<sub>2</sub> via C(sp<sup>2</sup>)-H functionalization, yielding pyridone-3-carboxylic acids, which are valuable biorelevant compounds. Importantly, Cu(I)@Zr-MOF maintained excellent performance over several cycles, preserving both its catalytic efficiency and chemical stability. Furthermore, theoretical calculations elucidated the detailed mechanism of the Cu(I)@Zr-MOF-catalyzed conversion of CO<sub>2</sub> into propionic acids and pyridone-3-carboxylic acids. This study presents a sustainable approach for a Cu(I) metal-based catalyst that effectively utilizes CO<sub>2</sub> for the carboxylation of unreactive C(sp)-H and C(sp<sup>2</sup>)-H bonds, rendering valuable chemicals such as propionic acids and pyridone-3-carboxylic acids under environmentally friendly conditions.</p>
51.	<p><a href="#">Numerical investigation on toxicity potential of PAHs emitted from hydrogen-diesel fueled dual-fuel engine</a>  <b>NK Yadav, MR Saxena, RK Maurya - Environmental Science and Pollution Research, 2025</b></p> <p><b>Abstract:</b> This study numerically investigates the effect of exhaust gas recirculation (EGR) and fuel-premixing ratio on the PAH emissions (naphthalene, benzo[a]pyrene, phenanthrene, acenaphthene, pyrene, benzo perylene, chrysene, and benzo [g,h,i]perylene), its precursors (such as C<sub>2</sub>H<sub>3</sub>, C<sub>2</sub>H<sub>2</sub>, C<sub>4</sub>H<sub>5</sub>, C<sub>4</sub>H<sub>3</sub>, C<sub>6</sub>H<sub>5</sub>, C<sub>6</sub>H<sub>6</sub>), and their toxicity potential from conventional diesel and hydrogen/diesel dual-fuel (HDDF) engine. The aim of this investigation is to understand the effect of EGR mass fraction and hydrogen energy share (HES) on the toxicity potential of PAHs and total PAH mass emission in conventional diesel and dual-fuel combustion under different loading conditions. This study is focused on the thermal, chemical, and dilution effects of EGR with and without HES on PAH formation. The simulations are performed on ANSYS Forte using a detailed chemical mechanism of diesel surrogate (66.8% n-decane/33.2% alpha-methylnaphthalene). The reaction mechanism used for simulation consists of 189 species and 1392 reactions. Results demonstrate that as the EGR increases from 10 to 30% in conventional diesel combustion, the toxicity equivalent potential of PAHs increases by 25% at lower engine load. However, at a fixed engine load and a constant EGR level of 30%, increasing the hydrogen energy share (HES) to 30% results in a 33% reduction in the toxicity equivalent potential of PAHs. This reduction highlights the potential benefits of hydrogen addition alongside EGR in future hydrogen–diesel dual-fuel engines. Additionally, the incorporation of hydrogen significantly reduces the mass emission of PAHs.</p>



52.	<p><a href="#">Ohmic contact to Schottky conversion for mitigating the oxygen defects present at the Ni/MgO-Ga<sub>2</sub>O<sub>3</sub> interface</a>  Shivani, RB Marathe, AG Chakkar...M Kumar - Journal of Physics D: Applied Physics, 2025</p> <p><b>Abstract:</b> Gallium oxide (Ga<sub>2</sub>O<sub>3</sub>) holds significant potential for next-generation power devices with its intrinsic capability to hold a higher electric field than conventional semiconductors before its breakdown. However, the operation of Ga<sub>2</sub>O<sub>3</sub>-based power devices and their figure-of-merit are significantly influenced by the quality of metal-Ga<sub>2</sub>O<sub>3</sub> contacts and interface defects. Here, we report the influence of oxygen vacancies on the electronic properties of Ni/MgO-Ga<sub>2</sub>O<sub>3</sub> metal-oxide-semiconductor interfaces. We explore the interface between Ga<sub>2</sub>O<sub>3</sub> and a thin MgO layer with variable oxygen vacancies for Schottky barrier diodes (SBDs). A Ni/MgO-Ga<sub>2</sub>O<sub>3</sub> stack with 0% oxygen flow during MgO growth offers a rather leaky (ohmic) characteristic owing to the existence of oxygen defects at the Ni/MgO-Ga<sub>2</sub>O<sub>3</sub> interface. However, for MgO film with 66% oxygen flow during its growth, the Ni/MgO-Ga<sub>2</sub>O<sub>3</sub> SBD exhibits a rectifying behaviour as a result of the compensated oxygen vacancies. X-ray photoelectron spectroscopy and frequency-dependent capacitance-voltage and conductance-voltage characteristics were analysed to elucidate the mechanisms of the transition from ohmic to Schottky behaviour of the contact. This study paves the way for understanding and controlling interface defects, which are essential for advancing the development of next-generation power electronics.</p>
53.	<p><a href="#">Pattern transitions and nonmonotonic changes in finger width due to the flow rate in partially miscible viscous fingering</a>  RX Suzuki, T Ban, M Mishra, Y Nagatsu - Physical Review E, 2025</p> <p><b>Abstract:</b> The displacement of a viscous fluid by another less-viscous fluid in porous media or Hele-Shaw cells produces a fingerlike interfacial pattern known as viscous fingering (VF). Classically, the dynamics of VF have been divided into two categories depending on whether the two fluids are fully miscible or immiscible. However, very recently, attention has been drawn to a third category of VF: VF in partially miscible systems. Our previous experimental study showed that the VF pattern in a partially miscible system transforms into a multiple droplet pattern due to phase separation and that the droplets spontaneously move. Here, we experimentally investigate the effect of the flow rate on VF in a partially miscible system. We show that multiple droplets are suppressed and a viscous finger-dominated pattern in which the fingers are wider than those of the corresponding immiscible VF is formed under an intermediate flow rate. For a large flow rate, the typical finger width is similar to that of the corresponding immiscible VF. As a result, we identify a nonmonotonic relation between the finger width and the flow rate (or capillary number), which is not observed in fully miscible and immiscible systems and is a specific characteristic of partially miscible systems. We elucidate the mechanism behind these observations based on an area measurement of the less-viscous solution and a velocity measurement of the spontaneous movement of the droplets. In addition, a numerical simulation for VFs in the partially miscible system can reproduce the suppression of the droplet formation and the finger widening, which are observed in the experiment with low and intermediate flow rate, and also show that the finger width becomes constant with Pe at high flow rates or seems to decrease with Pe, which implies that the increase in finger width can be suppressed with an increase in Pe. Moreover, the numerical simulation can support the validity of the mechanism discussed in the experimental part.</p>

54.	<p><a href="#">Performance enhanced copper-graphene hetero interconnect structures in crossbar arrays for neuromorphic computing</a>  <b>S Kushwaha, CB Rao, PR Shamini, S Roy, R Sharma - IEEE Journal on Multiscale and Multiphysics Computational Techniques, 2025</b></p> <p><b>Abstract:</b> In this paper, novel copper graphene heterogeneous interconnect structures are proposed which retain the ease of fabrication while having far better electrical performance when compared to the conventional copper interconnects. In the nanoscale regime, signal integrity (SI) of the copper interconnects degrades significantly. To address the signal integrity issues, these heterogeneous interconnects are developed at 7nm technology nodes which are further used to make the crossbar arrays for neuromorphic computing. The proposed copper graphene heterogeneous interconnects were designed by stacking the layers of copper and multilayer graphene nanoribbons (MLGNRs) one over the other and a detailed signal integrity analysis is done based on the quantities like the per unit length Resistance, Insertion Loss (IL), Return Loss (RL), eye diagrams, surface charge density and volume current density. The results shows that the proposed interconnects outperformed the copper interconnects based on each and every SI quantity. Finally, in the application example, the best performing heterogeneous interconnects are used to create larger crossbar arrays with sizes 64x64, 128x128. Further, the key performance matrices such as the delay time, the rise time and the fall time are analyzed and compared with the conventional crossbars made from the copper interconnects. The results in application example proved that the heterogeneous interconnects performs better than the copper interconnects for neuromorphic computing.</p>
55.	<p><a href="#">Power efficient range extension techniques for cattle health monitoring application</a>  <b>R Raina, KJ Singh, S Kumar - IEEE Journal of Radio Frequency Identification, 2025</b></p> <p><b>Abstract:</b> Monitoring cattle behavior regularly is essential for early detection of illness, stress or unusual activity. Although many cattle health monitoring systems exist in the literature, they often overlook techniques that balance power efficiency with range extension. Thus, this paper proposes Bluetooth Low Energy (BLE) based power efficient range extension techniques. These methods include designing high gain antennas for both the transmitter and receiver, using retransmissions and integrating a Power Amplifier (PA) at the transmitter and a Low Noise Amplifier (LNA) at the receiver. By optimizing the PA's transmission power and utilizing an LNA, the system achieves a communication range of upto approximately 2.5 km while conserving power. Moreover, a key novelty of this work is the smart power control mechanism that fine tunes the PA's output at the end node, providing an effective balance between the extended range and reduced power usage-an area that has been largely overlooked in existing BLE based cattle monitoring solutions.</p>
56.	<p><a href="#">Predicting cortical bone resorption in the mouse tibia under disuse conditions caused by transient muscle paralysis</a>  <b>H Shekhar, S Singh, J Prasad - Scientific Reports, 2025</b></p> <p><b>Abstract:</b> Load removal from the load-bearing bone, such as during extended space travel or prolonged bed rest, negatively affects bone health and leads to significant bone loss. However, the underlying principle that relates the bone loss to the lack of physiological loading is poorly understood. This work develops a mathematical model that predicts cortical bone loss at three sections along the length of a mouse tibia: distal, mid-section, and proximal. Dissipation energy density induced by loading, based on interstitial fluid flow, has been adopted as the mechanotransduction-triggering stimulus. The developed model uses the loss of stimulus due to the disuse of bone as an input and predicts the quantity of bone loss with spatial accuracy. It is hypothesized that the bone loss would occur at the site of maximum stimulus loss due to disuse. To test the hypothesis, stimulus loss was calculated, i.e., loss of dissipation energy density due to bone disuse, through poroelastic analysis using the finite element method. A novel mathematical model has been developed, successfully relating this loss of stimulus to the in vivo bone loss data in the literature. As per the model, the site-specific mineral resorption rate is shown to be</p>

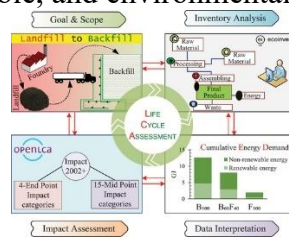
	<p>proportional to the square-root of the loss of dissipation energy density. To the best of the authors' knowledge, this model is the first of its kind to compute site-specific bone loss. The developed model can be extended to predict bone loss due to other disuse conditions, such as long space travel and prolonged bed rest.</p>
57.	<p><a href="#">Proton beam energy calibration of the 3 MV Tandetron™ at IFIN-HH</a>  DA Testov,... R Roy...V Vasilka... - Journal of Instrumentation, 2025</p> <p><b>Abstract:</b> The ELIGANT-TN long neutron counter, the ELISSA silicon strip array and the Mini-eTPC active gas target detector all represent nuclear physics research tools constructed at Extreme Light Infrastructure - Nuclear Physics (ELI-NP) for use in <math>\gamma</math>-beam experiments. Currently, these three setups are used at the charged particle accelerators of the “Horia Hulubei” National Institute for R&amp;D in Physics and Nuclear Engineering (IFIN-HH), for performing reaction cross-section measurements. Accurate knowledge of the incident beam energy is of paramount importance for such studies, which is why in the present article we report on a new proton beam energy calibration performed using the following threshold reactions: <math>{}^7\text{Li}(p,n){}^7\text{Be}</math>, <math>{}^{13}\text{C}(p,n){}^{13}\text{N}</math> and <math>{}^{51}\text{V}(p,n){}^{51}\text{Cr}</math>. The measurements were performed by varying the projectile energy across the key range of <math>\sim 1600</math>-<math>3200</math> keV. The results demonstrate a linear dependence of the projectile energy on the terminal voltage.</p>
58.	<p><a href="#">QbD-driven extraction and purification of piceatannol from passion fruit seeds and its cubosomes development, characterization, and neuronal cellular analysis</a>  N Soni, S Jat, A Gulbake, M Bhatt, B Das... - Food Bioscience, 2025</p> <p><b>Abstract:</b> Passion fruit (<i>Passiflora edulis</i>) is a tropical fruit widely recognized for its nutritional and medicinal properties, with its seeds being an underutilized source of bioactive compounds. Among these, piceatannol (PIC), a naturally occurring stilbene, has garnered significant attention due to its potent antioxidant, anti-inflammatory, and neuroprotective properties, among others. The purity, higher cost, and lower solubility or bioavailability challenges restricted the marketed potential of such therapeutics. To address these challenges, the study aims to develop a highly efficient extraction method using a Quality by Design (QbD) approach to extract highly yielded and purified PIC from passion fruit seeds. The QbD framework systematically identified and optimized critical process parameters (CPPs) and critical quality attributes (CQAs) to successfully optimize the process parameters. Furthermore, to encounter the lower bioavailability challenges or to achieve therapeutic applications from PIC, PIC-loaded cubosomes (PIC-CBs) were developed and characterized using various techniques. PIC-CBs possess <math>96.25 \pm 5.23</math> nm sized monodisperse particles with an encapsulation efficiency of <math>81.58 \pm 1.24</math> %. In-vitro release study results demonstrated a biphasic release pattern with sustained drug release for up to 24 h, required to produce a longer therapeutic effect. The developed PIC-CBs depicted the non-hemolytic blood profile, explaining the biocompatibility. Neuronal cellular analysis using PC-12 cells demonstrated the neuroprotective potential of PIC-CBs against oxidative stress-induced neuronal damage. The findings emphasize the promise of passion fruit seeds as a valuable source of PIC and the potential of cubosomes as a novel drug delivery system for neurodegenerative Alzheimer's disease interventions.</p> 
59.	<p><a href="#">Reconfiguration and locomotion with joint movements in the Amoebot model</a>  A Padalkin, M Kumar, C Scheideler - Autonomous Robots, 2025</p> <p><b>Abstract:</b> We are considering the geometric amoebot model where a set of namoebots is placed on the triangular grid. An amoebot is able to send information to its neighbors, and to move via expansions and contractions. Since amoebots and information can only travel node by node, most</p>

	<p>problems have a natural lower bound of where <math>D</math> denotes the diameter of the structure. Inspired by the nervous and muscular system, Feldmann et al. (Computat Biol 29(4):317–343, 2022) have proposed the reconfigurable circuit extension and the joint movement extension of the amoebot model with the goal of breaking this lower bound. In the joint movement extension, the way amoebots move is altered. Amoebots become able to push and pull other amoebots. Feldmann et al. (Computat Biol 29(4):317–343, 2022) demonstrated the power of joint movements by transforming a line of amoebots into a rhombus within rounds. However, they left the details of the extension open. The goal of this paper is therefore to formalize and extend the joint movement extension. In order to provide a proof of concept for the extension, we develop centralized algorithms for two fundamental problems of modular robot systems: reconfiguration and locomotion. We approach these problems by defining meta-modules of rhombical and hexagonal shape, respectively. The meta-modules are capable of movement primitives like sliding, rotating, and tunneling. This allows us to simulate reconfiguration algorithms of various modular robot systems. Finally, we construct three amoebot structures capable of locomotion by rolling, crawling, and walking, respectively.</p>
60.	<p><a href="#">Revisiting slope stability analysis using tension-truncated power-law yield criterion</a>  <b>R Ganesh</b> - International Journal for Numerical and Analytical Methods in Geomechanics, 2025</p> <p><b>Abstract:</b> Existing studies on slope stability have mostly been performed using the linear yield criterion without accounting for the true tensile strength of soils. However, soils generally exhibit marked nonlinearity in shear strength and practically negligible tensile strengths compared to theoretical estimates from the yield function. This research revisits the finite slope stability problem under plane strain conditions by employing a power-law (PL) yield criterion with a tensile strength cut-off. Here, a PL yield criterion is truncated with a circular stress envelope that tangentially encompasses the nonlinear PL yield function for a given uniaxial tensile strength. Unlike earlier studies, this research proposes a new horizontal slice-based rotational failure mechanism, and the solutions are rigorously determined within the upper bound plasticity theory by fully accounting for the variable nature of friction angles along the slip surface in a nonlinear bonded medium. The effect of pore-water pressure on the results is also investigated. The study shows that additional nonlinearity in the yield function, due to the tensile strength cut-off, can significantly influence the outcome of the stability assessment. The results of this study compared reasonably well with findings in the existing literature. The novelty of this study lies in presenting a new slice-based numerical solution procedure for investigating slope stability with variable friction angles and demonstrating the significant impact of tensile strength cut-off on stability assessment outcomes in nonlinear bonded soils.</p>
61.	<p><a href="#">Selective ring-opening of furfuryl alcohol to 1, 5-pentenediol over Pt/aluminosilicates</a>  <b>LJ Dumdell...A Shivhare, JA Hunns...</b> - RSC Sustainability, 2025</p> <p><b>Abstract:</b> Biomass-derived diols are key chemical building blocks for the sustainable chemical manufacturing of textiles and plastics, however their synthesis by a selective, scalable process from holocellulose is challenging. Furfuryl alcohol (FALC) is a potential precursor to 1,5-pentenediol (1,5-PeD) through acid-catalysed hydrogenolysis, and hence the impact of oxide support acidity on this reaction over Pt nanoparticles was investigated under batch and continuous flow in toluene. Platinum dispersed over weakly acidic fumed silica and mesoporous SBA-15 supports was almost inactive towards furfuryl alcohol at 150 °C and 10 bar H<sub>2</sub> and promoted decarbonylation and hydrodeoxygenation of FALC to furan and methyltetrahydrofuran, respectively. The introduction of Al<sup>3+</sup> into silica supports, to form either an amorphous silica-aluminate (ASA) or mesoporous Al-SBA-15, selectively activated the cyclic ether bond at the C2-O position, increasing the specific activity for FALC conversion in continuous flow from 20 mmol g<sub>Pt</sub><sup>-1</sup> h<sup>-1</sup> (Pt/SBA-15) to 295 mmol g<sub>Pt</sub><sup>-1</sup> h<sup>-1</sup> (Pt/ASA), and 1,5-PeD selectivity from ~25% (Pt/SBA-15) to 65% (Pt/ASA). This synergy between metal and acid sites resulted in a &gt;25-fold enhancement in 1,5-PeD productivity, reaching 186 mmol g<sub>Pt</sub><sup>-1</sup> h<sup>-1</sup> for Pt/ASA, and was maintained for 7 h time-on-stream with negligible deactivation or metal leaching. A moderately acidic Pt/γ-Al<sub>2</sub>O<sub>3</sub> catalyst exhibited reactivity intermediate between that of the Pt/silica and</p>



	<p>Pt/aluminosilicate catalysts. The yield of 1,5-PeD was directly proportional to the support acid site loading, indicating a common reaction mechanism. These findings demonstrate the striking promotion of metal catalysed hydrogenation that can be achieved through judicious support selection, and its translation from batch to flow with similar reaction kinetics.</p>
62.	<p><a href="#">Space-time fractional diffusion with stochastic resetting</a>  <b>Priti, A Kumar</b> - <i>Statistics &amp; Probability Letters</i>, 2025</p> <p><b>Abstract:</b> In this article, we study the space–time fractional diffusion equation (STFDE) which is a generalization of the classical diffusion equation, in the presence of stochastic resetting. The STFDE is formulated by replacing the standard time and space derivatives with the Caputo and Riesz fractional derivatives, respectively, to capture anomalous diffusion behaviors. We derive analytical solutions using Laplace and Fourier transforms, and express them in terms of Fox H-functions. We obtain a closed-form expression for the stationary distribution and prove the finiteness of the mean first passage time. Additionally, we examine how stochastic resetting influences the infinite divisibility of the standard diffusion process, showing that this property is lost once resetting is introduced. The reset mechanism interrupts the Lévy process at random times, effectively altering the jump structure and destroying the self-decomposability required for infinite divisibility.</p>
63.	<p><a href="#">Surface charge effects on Sr-hydroxyapatite degradation in water solution: Surface and penetration diffusion</a>  <b>J Wen...R Ahuja, Z Zhang</b> - <i>Journal of the American Ceramic Society</i>, 2025</p> <p><b>Abstract:</b> Hydroxyapatite (HAP) can serve as a critical permeable reactive barrier for the in situ remediation of <sup>90</sup>Sr radionuclides from groundwater through promoting co-precipitation. The Sr<sup>2+</sup> leaching associated with the structural degradation of Sr-HAP in the geological field environment is crucial for lowering groundwater radioactivity; thus, evaluating HAP chemical durability is critical. However, the degradation mechanism of Sr-doped HAP upon water solutions under the influence of surface charge effects remains unclear and requires further investigation. In this work, the surface degradation and penetration diffusion of Sr-doped HAP are systematically investigated based on density functional theory and dissolution experiments. Some specific issues such as the preparation process of single-phase ceramics and surface morphology are discussed in details, along with uncovering the relationship between Sr–O bond and Sr leaching activity. The results reveal that the degradation behavior of Sr-HAP ceramics follows a typical dissolution-precipitation process. The presence of unsaturated chemical bonds derived from incomplete [SrO<sub>7</sub>] and [SrO<sub>9</sub>] coordination polyhedra can enhance the ability of Sr-HAP to facilitate surface adsorption and contribute to the nonuniform distribution of electronic states at the nanoscale. Importantly, the hydrogen bonds from aqueous solution provide a strong upward pulling force for the surface adsorption sites to render the metastable surface structure rather than water molecule penetration diffusion, leading to the outer layer of the (0 0 1) surface spontaneously twists to form Schottky defects.</p>
64.	<p><a href="#">Sustainability evaluation of waste foundry sand as backfill in cantilever retaining walls</a>  <b>A Kumar, A Parihar</b> - <i>Geomechanics and Geoengineering</i>, 2025</p> <p><b>Abstract:</b> This study investigates the life cycle environmental impact of using waste foundry sand (WFS) as backfill material for cantilever retaining walls. Life Cycle Assessment (LCA) methodology compares the environmental footprint of WFS backfill with conventional sand backfill. The openLCA software tool is utilised along with the Ecoinvent v3.8 database. A functional unit of a 1-metre-long and 3-metre-high retaining wall construction is established. The IMPACT 2002+ method assesses the environmental impact across various mid-point categories. It is found that the use of WFS and the optimal sand-WFS mixture reduces the renewable and non-renewable energy demand by 89.14% and 37.58%, respectively, and decreases the environmental impact in all 15 mid-point impact categories. Concrete production and sand mining are found to be significant contributors in all categories and cases. The cost of the construction of the wall with</p>

WFS backfill was also reduced by 63%. This study indicates that the use of WFS backfill is technically feasible, socially acceptable, and environmentally beneficial.



[Taming instability: Scaffold like polyaniline for enhancing the sedimentation stability and their influence on stability-magnetization tradeoff in viscoelastic magnetorheological fluids](#)

R Sharma, S Sinha, N Ali, R Singh, V Mehandia... - Physics of Fluids, 2025

65.

**Abstract:** Magnetorheological fluids (MRFs) rely on the dynamic interplay of magnetic interaction, particles dispersion, and viscoelastic response, yet achieving long-term sedimentation stability without significantly compromising magnetic properties remains a significant challenge. This study introduces a pioneering strategy by employing polyaniline (PANI) as a scaffold-like additive to bolster the sedimentation stability of Fe-based MRFs. The high surface area and porous architecture of PANI foster a supportive network that evidently enhances particle dispersion, achieving a sedimentation ratio of 44.0% at an optimal 2 wt. % PANI concentration—more than doubling the stability of bare Fe-based MRFs (20.9%). Brunauer–Emmett–Teller (BET) surface area analysis confirms that PANI's porous morphology (~24× higher pore volume than Fe) facilitates enhanced particle dispersion and steric stabilization, mitigating gravitational settling. This investigation elucidates the nuanced trade-off between sedimentation stability and magnetic properties, offering a physics-driven framework to optimize MRFs for practical applications. The incorporation of non-magnetic PANI introduces a deliberate trade-off, wherein enhanced colloidal stabilization and steric hindrance come at the expense of reduced magnetic coupling efficiency and field-induced dipolar interactions. While the saturation magnetization ( $M_s$ ) reduces from 218 emu/g (Fe) to 71.4 emu/g (Fe with 4 wt. % PANI) due to particle dilution and increased interfacial porosity, the magneto-yield stress remains sufficiently high—decreasing from 941 to 438 Pa at  $H = 123$  kA/m—preserving functional field-responsiveness. Oscillatory shear analysis reveals that storage modulus ( $G'$ ) attains  $2.22 \times 10^5$  Pa at 123 kA/m for FeP 2%, with  $\tan \delta < 0.20$  in the linear viscoelastic regime, indicating a strongly elastic character necessary for dissipative control applications. The flow behavior transitions into a pronounced shear-thinning regime ( $n \sim 0.706\text{--}0.952$ ), which aligns with the breakdown of anisotropic field-induced structures under strain. This rheo-magnetic trade-off between PANI-induced stabilization and reduction in magneto-mechanical coupling is carefully optimized, yielding MRFs with sufficient magnetic actuation and improved structural fidelity. The insights provided herein offer a robust structure-property framework for designing application specific MRFs, where sedimentation stability, magnetic tunability, and rheological integrity must be simultaneously addressed.

66.

[The role of activity in the nonlinear rheology and flow processes of active fiber \(\*Turbatrix aceti\*\) suspensions](#)

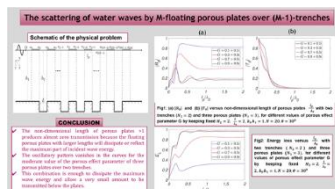
N Ali, M Mishra, V Mehandia - Physics of Fluids, 2025

**Abstract:** Nematodes, with their active motility and fiber-like structure, serve as excellent models for studying active fluid behavior. This study explores the nonlinear rheology of active and inactive *Turbatrix aceti* suspensions using large amplitude oscillatory shear experiments and applying the sequence of physical processes method to assess Cole–Cole plots and Trefoil profiles in addition to storage and loss moduli ( $G'$  and  $G''$ ) and loss factor [ $\tan(\delta)$ ] to explore the interplay between activity-induced and externally applied flow effects. At low frequencies, active suspensions display a stable viscoelastic state [ $G' \approx G''$ ] without crossover, transitioning to a viscous regime at higher strain amplitudes. Inactive/passive suspensions, in contrast, exhibit viscoelastic gel-like behavior ( $G' > G''$ ) with clear crossover points. The transition points shift to lower strains at higher frequencies for both active and passive suspensions. At  $f=4$ , which

matches with the nematode's natural undulation frequency (4–6 ), active and passive suspensions display similar viscous behavior, indicating that the influence of nematode activity is effectively suppressed by the external flow field. Our study shows that higher frequencies reduce the applied shear strain threshold required to overcome nematode-driven activity, with external power dominating at  $f=4$  . These findings advances our understanding of activity–flow interactions in complex fluids and lays the groundwork for practical applications, such as the design of nematode-inspired microrobots, microfluidic mixers, and design of on-demand flow generating systems for medical and industrial applications.

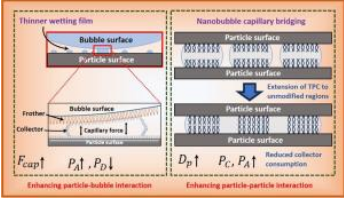
67. [The scattering of water waves by  \$M\$ -floating porous plates over  \$\(M - 1\)\$  trenches](#)  
**S Choudhary, SC Martha, T Sahoo** - *Journal of Offshore Mechanics and Arctic Engineering*, 2025

**Abstract:** This article investigates the interaction of water waves with multiple thin horizontal floating porous plates over multiple trenches at the bottom. Here, the horizontal floating porous plates are placed at a finite distance from each other, and the trenches are in between the plates. Using the linearized theory of water waves, the boundary value problem is solved for velocity potential using Havelock’s expansion and algebraic least-square method. To understand the advantage of multiple porous plates and trenches, the numerical results are plotted for the scattering and dissipation coefficients through different graphs to examine the effect of various parameters. In the direction of the use of a minimal number of porous plates in the absence of trenches, it is observed that the curves almost coincide for the three and four-plate cases, implying three plates will be sufficient for maximum wave energy dissipation and minimal wave transmission. But, for the case of two trenches and in the absence of porous plates, the curves show an oscillatory pattern with harmonic and subharmonic peaks. The study also shows that the oscillating pattern in the curves vanishes when there are two trenches and three porous plates with moderate values of the porous-effect parameter. In the latter case, plates with larger lengths will produce almost zero transmission and dissipate or reflect a major part of the incident wave energy. It is concluded that the above-specific combination of barriers and plates dissipates maximum wave energy and transmits a small amount, providing a safer zone in the trench regions. Thus, multiple navigation channels can be created to overcome the issues of dense vessel traffic arising in a single channel.



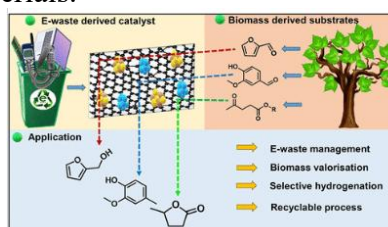
68. [Towards an RGB camera-based rehabilitation exercise assessment using an enhanced spatio-temporal transformer framework](#)  
**A Chander, DR Bathula, AK Sahani** - *Multimedia Tools and Applications*, 2025

**Abstract:** Rehabilitation following surgery or trauma is crucial for patient recovery. However, many patients attempt to rehabilitate at home by performing exercises without professional supervision, potentially hindering their progress or causing complications. To address this, deep learning systems have been extensively explored. Traditional motion detection systems such as Vicon or Kinect, while effective, are costly or impractical for at-home use. Therefore, leveraging the ubiquity of mobile devices, we propose an affordable and robust home-based rehabilitation system that uses a simple RGB camera for recording physical exercises. We used Mediapipe, an open-source framework, to extract joint coordinate information from video frames. Our spatio-temporal transformer encoder model is enhanced with dual attention and weighted residual connections for assessing human motion quality using skeleton data. Our model has been evaluated on a custom RGB dataset, as well as two benchmark datasets—UI-PRMD and KIMORE, and achieves state-of-the-art performance in motion quality assessment, demonstrating an average reduction of 12.9% in mean absolute error (MAE) across all datasets. Our approach has the

	<p>potential to be a cost-effective and reliable solution for home-based rehabilitation, offering advanced motion assessment capabilities without the need for expensive equipment.</p>
69.	<p><a href="#">Ultrabroadband nonlinear Hall rectifier using SnTe</a>  <b>F Hu...</b> <b>R Sharma, G Eda...</b> - <i>Nature Nanotechnology</i>, 2025</p> <p><b>Abstract:</b> The rapid expansion of self-powered electronics in the Internet of Things, 6G communication and millimetre-wave systems calls for rectifiers capable of operating across ultrabroadband frequencies and at extremely low input power levels. However, conventional rectifiers based on semiconductor junctions face fundamental limitations such as parasitic capacitance and threshold voltages, preventing effective operation under broadband and ambient radio-frequency conditions. Here we present an ultrabroadband, zero-bias rectifier based on the nonlinear Hall effect in wafer-scale (001)-oriented topological crystalline insulator SnTe thin film. This material exhibits a large second-order conductivity of <math>\sim 0.004 \Omega^{-1} \text{V}^{-1}</math>, surpassing that of other wafer-scale materials. The nonlinear Hall effect arises primarily from a Berry curvature dipole, evidenced by angular-resolved transport measurements and first-principles calculations. The device demonstrates rectification from 23 MHz to 1 THz, with sensitivity down to <math>-60 \text{ dBm}</math> in key radio-frequency bands, without any external bias. Rectified output power is scalable through series- and parallel-array topologies and can be enhanced using rectenna designs. As a proof of concept, we achieve the wireless powering of a thermistor using harvested radio-frequency energy, validating the potential of this material platform and nonlinear Hall effect for next-generation energy-autonomous microsystems.</p>
70.	<p><a href="#">Understanding the role of nanobubbles on reducing collector and frother dosages in fine particle flotation</a>  <b>N Dutta, H Sharma, G Yadav, N Nirmalkar, S Mitra</b> - <i>Separation and Purification Technology</i>, 2025</p> <p><b>Abstract:</b> Bubble-particle interactions critically control the recovery kinetics of the flotation process, which is widely encountered in various industrial and environmental separation applications. Although widely used, the process has known limitations in handling fine particles (<math>&lt;30 \mu\text{m}</math>) due to their low inertia. In the present study, we examined the potential use of nanobubbles to improve the flotation performance of fine particles while simultaneously minimizing the consumption of flotation reagents, which included collector and frother chemicals. Nanobubble suspension with a greater bubble number density was demonstrated to improve the total flotation recovery of fine particles by up to 11%. Whereas the collector and frother concentrations were reduced by approximately 50% and 60%. On the other hand, nanobubbles significantly reduced the overall size of the floated particles by up to 58%, suggesting that a greater number of finer particles were collected. It is hypothesized that capillary bridges are formed between the particles in the presence of nanobubbles, which result in the formation of aggregates. These aggregates, due to their increased inertia, form a stable three-phase contact with the relatively coarser size carrier bubbles at a faster rate, resulting in an enhanced recovery. Also, during the interparticle interactions, the nanobubble capillary bridges merge and extend the three-phase contact line, thereby increasing the attractive capillary force that compensates for the reduced hydrophobic interaction at low dosage of collector reagent.</p> 
71.	<p><a href="#">Upcycling waste electronic chips into metallic catalysts for sustainable biomass valorization into fuel additives and fine chemicals</a>  <b>A Chauhan, R Bal, R Srivastava</b> - <i>Industrial &amp; Engineering Chemistry Research</i>, 2025</p>



**Abstract:** The rapid growth of electronic waste (E-waste) poses significant environmental challenges and presents an opportunity for sustainable metal recovery. Addressing the gap in E-waste management and green catalyst development, this study repurposes waste electronic memory chips from old laboratory PCs to synthesize metal-based catalysts. Metals were extracted via acid leaching and supported on a composite of metal oxide ( $\text{CeO}_2$ ,  $\text{Al}_2\text{O}_3$ ,  $\text{SiO}_2$ ) and carbon derived from chitin (CHT), forming the  $\text{Cu}@MO/\text{CHT}$  catalyst. The  $\text{Cu}@CeO_2/\text{CHT}$  catalyst exhibited 100% selectivity in the hydrogenation of biomass-derived  $\text{C}=\text{O}$  compounds, including furfural, 5-hydroxymethylfurfural, vanillin, levulinic acid, ethyl levulinate, syringaldehyde, and N-heterocyclic compounds such as quinoline. The  $\text{Cu}@CeO_2/\text{CHT}$  catalyst was efficient at the millimole and the gram scale. XPS, Raman spectroscopy, and HRTEM analyses suggest the role of oxygen vacancies in  $\text{CeO}_2$ , promoting selective adsorption of  $\text{C}=\text{O}$  groups. Metal content in the E-waste leachate and catalyst was determined using MP-AES, and the catalyst maintained high activity over at least five consecutive cycles. Furthermore, the use of green solvents, such as ethanol, aligns the process with sustainable chemistry principles, minimizing environmental impact. This study demonstrates the dual benefits of E-waste recycling and green catalyst development, offering a pathway to sustainable biomass valorisation. This work addresses the global E-waste crisis and the need for eco-friendly, scalable catalytic processes by converting E-waste into valuable catalytic materials.

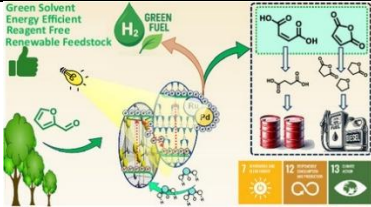


[Visible-light-driven additive-free photocatalytic oxidation of furfural to maleic acid and green hydrogen](#)

**R Ghalta, R Srivastava - ChemSusChem**

72.

**Abstract:** Developing additive-free photocatalytic systems capable of simultaneously valorizing biomass and producing green hydrogen under visible light remains a key challenge in sustainable chemistry. Herein, a  $\text{Pd}@\text{Ru}$  bimetallic Z-scheme photocatalyst ( $1.5\text{Pd}3\text{Ru}@OCN/\text{WO}_3$ ) that selectively oxidizes furfural while splitting water, yielding a hydrogen evolution rate of  $22.33 \text{ mmol g}^{-1} \text{ h}^{-1}$  and maleic acid with high productivity ( $6.69 \text{ mmol g}^{-1} \text{ h}^{-1}$ ) and selectivity (85%) is presented. The product selectivity between maleic acid and maleic anhydride can be precisely controlled by adjusting the solvent conditions. The performance of the catalyst is attributed to the decorated  $\text{Pd}@\text{Ru}$  alloy nanoparticles, which provide intimate contact and exploit the low Fermi level of metals for electron trapping and proton activation, confirmed by photoelectrochemical studies. The  $\text{OCN}/\text{WO}_3$  Z-scheme heterojunction facilitates directional charge migration, confirmed through Ultraviolet Photoelectron Spectroscopy (UPS), Valence Band X-ray Photoelectron Spectroscopy (VB-XPS), Mott–Schottky (MS), and in situ XPS analyses. Further investigation of charge dynamics using photoluminescence, electrochemical impedance spectroscopy, transient photocurrent measurements, and time correlated single photon counting reveals prolonged charge carrier lifetimes and reduced recombination. Electron Paramagnetic Resonance (EPR), DMPO spin-trapping, and Electrospray Ionization Mass Spectrometry (ESI-MS) studies elucidate a radical-mediated oxidation pathway involving  $\text{O}_2^{\bullet-}$ ,  $\bullet\text{OH}$ , and a key intermediate ( $\text{C}_5\text{H}_3\text{O}_2^{\bullet}$ ). A comprehensive green metrics assessment under batch process demonstrates excellent atom economy, low E-factor, and high material recovery, validating the catalyst's sustainability.

	
73.	<p><a href="#"><u>Wave attenuation on seawall by submerged thick porous structure over a step-type seabed</u></a>  <b>G Sahoo, SC Martha - Journal of Offshore Mechanics and Arctic Engineering, 2025</b></p> <p><b>Abstract:</b> This study presents a novel model that features a thick submerged porous structure (SPS) designed to protect a seawall in the presence of M steps at bottom. Using the governing equation and boundary conditions through the eigenfunction expansion method, a system of equations is obtained. The system is solved through MATLAB to determine the unknown coefficients. The numerical values of force, reflection coefficient and dissipation coefficient are obtained and plotted through graphs. The model is validated by comparing with literature results and verifying energy identity. Compared to the scenario without steps, the present study results in a 57% reduction force on the wall. In comparison to the problem without SPS, the present study observed a 26% reduction in the force on the wall. Observations suggest that varying the submergence depth (ranging from 0.1 to 0.3) and length (ranging from 0.1 to 0.6) of SPS leads to wave reflection and force on the wall approximately less than 54% and 59%, respectively. In particular, with a larger width of SPS, the influence of the height of the steps becomes negligible. With increasing porosity and frictional coefficient, the force on the seawall decreases. The force on the wall exhibits harmonic peaks at angles <math>\theta = 38^\circ</math> and <math>\theta = 61^\circ</math>, while <math>\theta = 67^\circ</math> is identified as the critical angle for the reflection and dissipation coefficients. These results are crucial for developing SPS, where surface-piercing structures hinder navigation and bottom-standing structures may not be fitted over an unstable bottom.</p>

**Disclaimer:** This publication digest may not contain all the papers published. Library has compiled the publication data as per the alerts received from Scopus and Google Scholar for the affiliation “Indian Institute of Technology Ropar” for the month of August, 2025. The author(s) are requested to share their missing paper(s) details if any, for the inclusion in the next publication digest.